(NASA-CR-162114) OCCULTATION STUDIES OF PLANETS AND SATELLITES: THE OCCULTATION OF EPSILON GEMINORUM BY MARS Final Technical Report, 1 Feb. - 31 Aug. 1976 (Cornell Univ., Ithaca, N. Y.) 30 p HC A03/MF A01 G3/91 N79-31121 Unclas 31753

CORNELL UNIVERSITY

Center for Radiophysics and Space Research

ITHACA, N. Y.

FINAL TECHNICAL REPORT

NASA GRANT NSG 7243

Occultation Studies of Planets and Satellites: The Occultation of ε Geminorum by Mars

Principal Investigator: Dr. James L. Elliot

Co-Investigators: Dr. Joseph Veverka

Dr. Carl Sagan

FINAL TECHNICAL REPORT

"Occultation Studies of Planets and Satellites: The Occultation of ϵ Geminorum by Mars"

NASA Grant NSG 7243
to Cornell University

Principal Investigator: Dr. James L. Elliot

Co-Investigators: Dr. Joseph Veverka

Dr. Carl Sagan

Grant Period: February 1, 1976 through August 31, 1976

Grant Amount: $16,420

The present grant was solicited to provide the supplemental funds needed to carry out observations of the occultation of the star ε Geminorum by Mars on April 8, 1976 with the Kuiper Airborne Observatory. This occultation occurred just three months before the Viking 1 entry into the Martial atmosphere and its subsequent landing on the Martian surface. The goals of the occultation observations were (i) to determine if the Martian atmosphere had large fraction argon, which would have caused damage to some of the Viking experiments; and (ii) to obtain temperature, pressure and number density profiles of the Martian upper atmosphere for direct comparison with the in-situ measurements of these quantities with the Viking data.

Successful photoelectric records of the occultation at high time resolution were obtained at three wavelengths simultaneously. A highlight of these observations was the unexpected discovery of the "central flash", which was observed when ε Gem was directly behind the center of Mars. The main results from this work are:

1. A measurement of the mean temperature of the Martian atmosphere about 145k at the 10^{-2}mbar pressure level (about 70km above the mean surface).
2. The discovery of wavelike temperature variations, which confirm the predictions of Zurek's tidal model.
3. The discovery of the "central flash", which we used to determine a normal optical depth of 0.23±0.11 for the

Martian atmosphere - a value in good agreement with subsequent Viking results.

4. Argon could not be the major constituent of the Martian atmosphere.

Further details of our observational procedures, methods of data analysis and our conclusions are contained in the reprints that follow the list of publications supported, in part, by this grant.

PUBLICATIONS

1. Scientific Papers:

"Occultation of ε Geminorum by Mars: Evidence for Atmospheric Tides?" Science (1977), 195, 485, by J.L. Elliot, R.G. French, E. Dunham, P.J. Gierasch, J. Veverka, C. Church, and Carl Sagan.

"Occultation of ε Geminorum by Mars. II. The Structure and Extinction of the Martian Upper Atmosphere", Astrophysical Journal (1977), 217, 661, by J.L. Elliot, R.G. French, E. Dunham, P.J. Gierasch, J. Veverka, C. Church, and Carl Sagan.

2. Abstracts of Papers Presented at Meetings:

"Structure of the Martian Upper Atmosphere from Airborne Observations of the Epsilon Geminorum Occultation", B.A.A.S. (1977), 9, 451 (also presented at the Division for Planetary Sciences Meeting, Honolulu, Hawaii, 19-22 January 1977) by J.L. Elliot, R.G. French, E. Dunham, P.J. Gierasch, J. Veverka, C. Church, and Carl Sagan.

"Martian Atmospheric Extinction and the Central Flash", B.A.A.S. (1977), 9, 415 (also presented at the Division for Planetary Sciences Meeting, Honolulu, Hawaii, 19-22 January 1977) by R.G. French, J.L. Elliot, P.J. Gierasch, E. Dunham, J. Veverka, C. Church, and C. Sagan.

3. Reports:

"The Occultation of ε Geminorum by Mars: A Pre-Viking Assessment of Results", a report submitted to the Viking project, June 1976 by J.L. Elliot, R.G. French, E. Dunham, P.J. Gierasch, C. Church, and C. Sagan.

4. Popular Articles:

"A Unique Airborne Observation", Sky and Telescope (1976), 52, 23 by J.L. Elliot, E. Dunham, and C. Church.

THE ASTROPHYSICAL JOURNAL, 217:661–679, 1977 October 15

OCCULTATION OF ϵ GEMINORUM BY MARS. II. THE STRUCTURE AND EXTINCTION OF THE MARTIAN UPPER ATMOSPHERE

J. L. ELLIOT, R. G. FRENCH, E. DUNHAM, P. J. GIERASCH, J. VEVERKA, C. CHURCH, AND CARL SAGAN
Laboratory for Planetary Studies, Cornell University
Received 1976 December 20; accepted 1977 April 13

ABSTRACT

The occultation of ϵ Geminorum by Mars on 1976 April 8 was observed at three wavelengths and 4 ms time resolution with the 91 cm telescope aboard NASA's G. P. Kuiper Airborne Observatory. Since most of the Earth's atmosphere was below the telescope, scintillation noise in the light curves was greatly reduced from that encountered by ground-based observers. Temperature, pressure, and number-density profiles of the Martian atmosphere were obtained for both the immersion and emersion events. Within the altitude range 50–80 km above the mean surface, the mean temperature is ~145 K, and the profiles exhibit wavelike structures with a peak-to-peak amplitude of 35 K and a vertical scale of about 20 km. The ratio of the refractivity of the atmosphere at 4500 Å and 7500 Å, determined from the time shift of the light curves for these wavelengths, is consistent with the atmospheric composition measured by *Viking 1*, 15 weeks later. From the "central flash"—a bright feature in the light curve midway between immersion and emersion—we find an optical depth at 4500 Å of 3.3 ± 1.7 per km atm (about 0.23 per equivalent Martian air mass) for the atmosphere about 25 km above the mean surface, near the south polar region. This large value and its weak wavelength dependence rule out Rayleigh scattering as the principal cause of the observed extinction.

Subject headings: occultations — planets: Mars — stars: individual

I. INTRODUCTION

The occultation of ϵ Geminorum ($m_v = +3.1$, G8 Ib) by Mars on 1976 April 8 was observed at three wavelengths with the 91 cm telescope aboard the Kuiper Airborne Observatory. A highlight of these observations was the discovery of the "central flash" when ϵ Gem was directly behind the center of Mars (Elliot, Dunham, and Church 1976). The records of the central flash yielded unexpected data on extinction in the Martian lower atmosphere—a new application for stellar occultation observations.

From the immersion and emersion light curves we have obtained temperature, pressure, and number-density profiles for the Martian atmosphere under the assumption that the density gradients are parallel to the gravity gradient. In the context of the β Scorpii occultation by Jupiter, the validity of this assumption has been disputed, and no evidence exists to settle the issue conclusively (Young 1976; Elliot and Veverka 1976; Jokipii and Hubbard 1977). The ϵ Gem occultation presents a unique opportunity to compare the structure and composition of the Martian upper atmosphere, obtained under the gravity-gradient assumption, with the in situ measurements made during the entry of *Viking 1*. A significant aspect of our analysis is the use of a new inversion technique (French, Elliot, and Gierasch 1977) that assigns error bars to the temperature, pressure, and number-density profiles.

II. OBSERVATIONS

Light curves of the occultation were obtained with our three-channel photometer (Elliot, Veverka, and Goguen 1975) attached to the bent Cassegrain focus of the 91 cm telescope aboard NASA's Kuiper Airborne Observatory (KAO). From the predictions by Taylor (1976*a*), the flight path was planned so that the apparent velocity of ϵ Gem was strictly perpendicular to the limb of Mars. This course was chosen to facilitate the analysis of the differential refractivity measurements (see § IV) but also resulted in the discovery of the "central flash" (see § V).

At the time of the occultation, the Martian subsolar latitude was $+19{.}^\circ2$ and the planetocentric longitude of the Sun (L_S) was $51{.}^\circ6$. Immersion occurred at about 0330 local Martian time above the suboccultation point 27° S and 331° W longitude. The suboccultation point for emersion was 28° N, 152° W longitude, and the event occurred at about 1530 local solar time.

According to the inertial navigation system on board the KAO, the telescope was located at latitude 35°26′.4 N and longitude 69°48′.0 W at immersion and latitude 36°04′.3 N and longitude 69°43′.3 W at emersion. The times for immersion ($00^h57^m19{.}^s68 \pm 0{.}^s04$ UTC) and emersion ($01^h02^m34{.}^s01 \pm 0{.}^s04$ UTC) are defined to be the "half-light" times obtained by fitting an isothermal light curve to the data (Baum and Code 1953). Errors in the telescope coordinates, owing to uncalibrated internal errors in the inertial

TABLE 1

MEAN WAVELENGTHS AND PASSBANDS

Channel No.	Mean Wavelength (Å)	Passband (FWHM, Å)†	$n_*/(n_♂ + n_*)$ (ratio of counting rates)	$\epsilon(\phi)$ Normalized rms Noise (for 1 s integration)
1................	3800‡	(150)	0.09	0.013
2................	4500	100	0.17	0.007
3................	7500	200	0.12	0.008

† Full width at half-maximum.

‡ The filter used had a center wavelength of 3700 Å, but the steep spectrum of ϵ Gem in this region must be accounted for before the mean wavelength for this channel can be known precisely. For the present we have adopted 3800 Å as the mean wavelength for this channel.

navigation system, are probably less than 2′. For both events the altitude of the plane was 12.5 km above sea level; its ground speed of 0.22 km s^{-1}, on a heading of 357°, was only 1% of the shadow velocity (21.9 km s^{-1}; Taylor 1976*a*).

The center wavelengths and passbands of the three photometric channels are given in Table 1. The photomultiplier for channel 1 had an S-4 photocathode response while those for channels 2 and 3 had an S-20 response. Each was contained in an uncooled, *rf*-shielded housing. Because of the large photon fluxes incident on the photomultipliers, voltage-to-frequency converters (Dunham and Elliot 1977) were used instead of pulse amplifiers. The alignments of the photomultipliers and their respective field lenses were carefully adjusted to make the photometer response independent of the position of a source within the entrance aperture of the photometer. Deviations from an ideal flat response could cause errors in the light curve in the event of poor telescope tracking. In fact, throughout the observations the telescope tracking was excellent, as confirmed by watching the image of Mars on a television screen that monitored a portion of the light received from a beam splitter within the photometer.

The data were recorded as a continuous series of 4 ms integrations, made simultaneously in all three channels, with a data-recording system described previously (Elliot, Veverka, and Goguen 1975). The data system clock was synchronized with time signals from radio station WWV when the KAO made its closest approach to Boulder, Colorado, a few hours before the occultation.

At the time of the occultation, both Mars and ϵ Gem were contained within an aperture 90″ in diameter. Continuous data recording began at 0030 and ended at 0116 UTC. A light curve of the entire event at 4500 Å is shown in Figure 1, at 1 s time resolution,

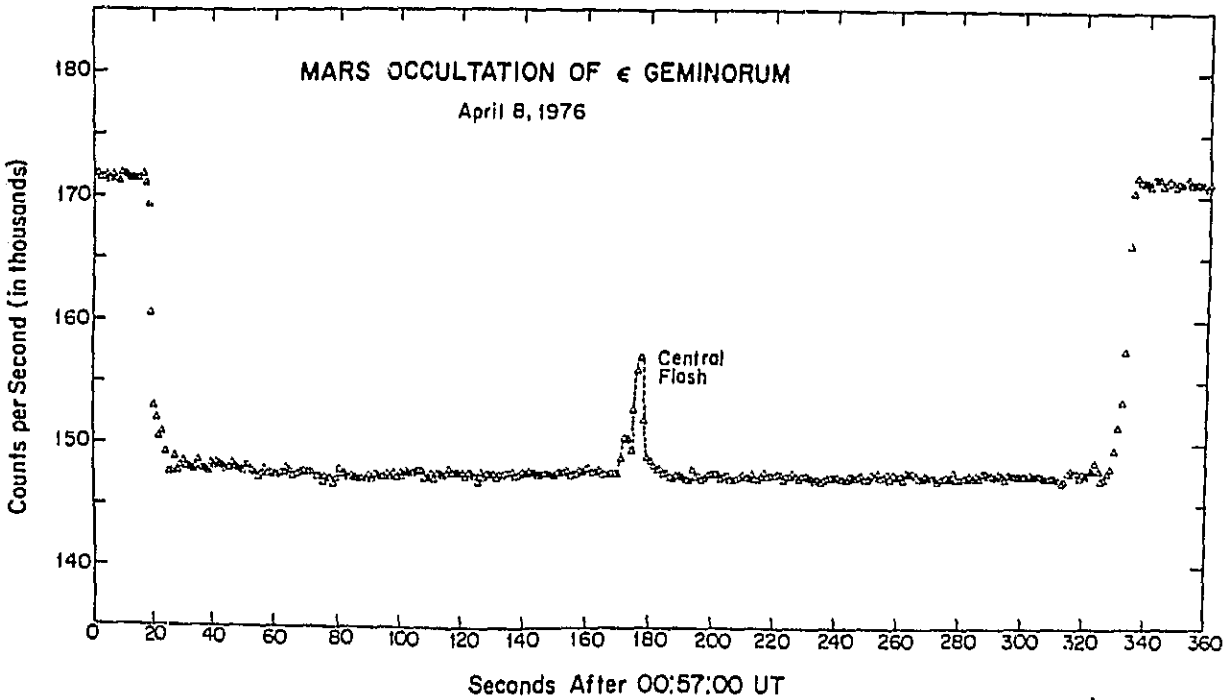

FIG. 1.—Light curve of the occultation obtained at 4500 Å; each point represents a 1 s integration. The central flash was produced by radially symmetric refraction when ϵ Gem was directly behind the center of the planet.

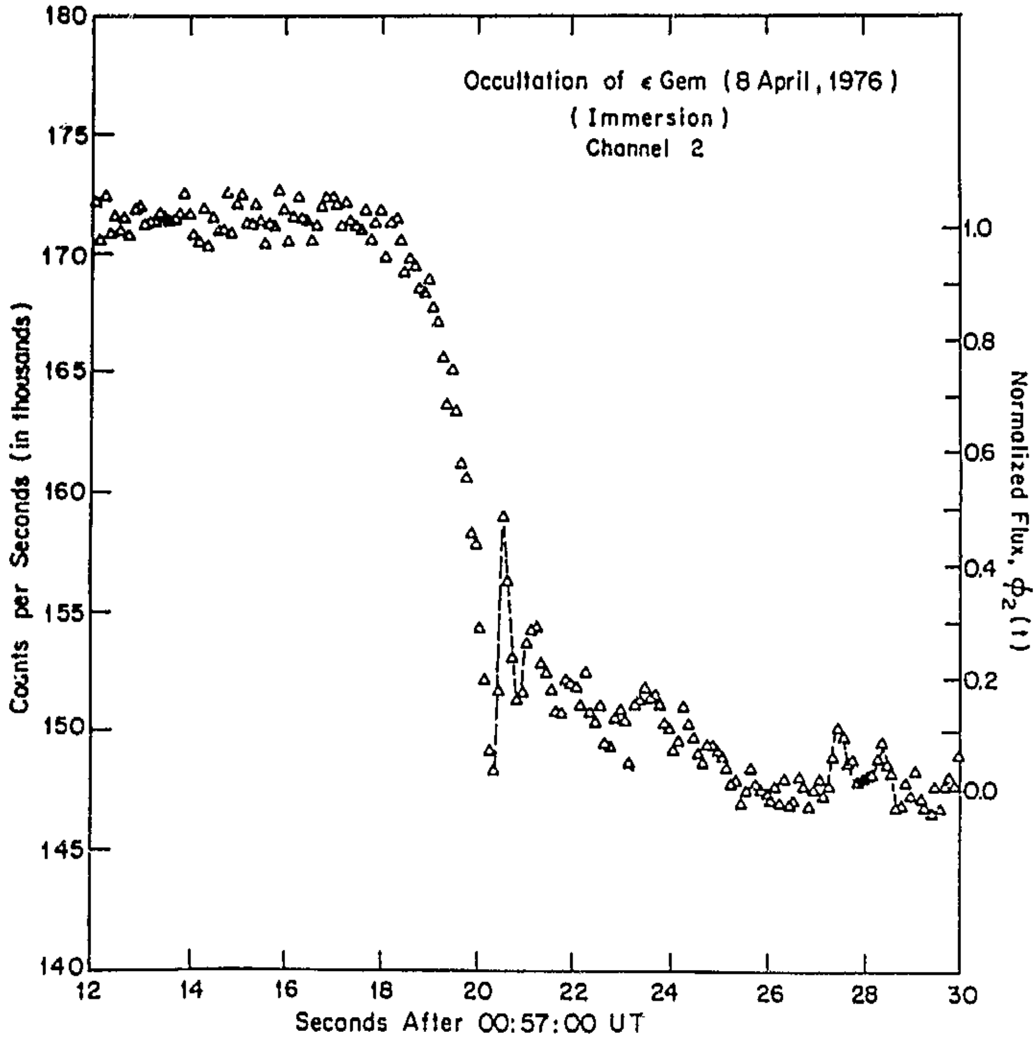

FIG. 2.—Immersion of ε Gem observed at 4500 Å; each point represents a 0.1 s integration. Prominent spikes are indicated by dashed lines.

where the central flash occurs exactly at mid-occultation. Figures 2 and 3 show light curves for immersion and emersion at 0.1 s time resolution. Spikes in the light curve are much less pronounced than for previous occultations by Neptune and Jupiter (Elliot and Veverka 1976), at least partially because of a large projected diameter of ε Gem at Mars (~6 km; de Vegt 1976).

Since our observations represent the first optical photometry performed with the airborne telescope, we shall briefly assess the photometric quality of the data. As seen in Figure 1, the baseline of the light curve is stable, showing little drift. The fourth column of Table 1 gives the ratio of the counting rate from ε Gem (n_*) to that from Mars ($n_♂$), and the background (n_b sky, dark counts, and v-to-f offset). For all channels $n_♂ \gg n_b$. The fifth column gives the rms noise in each channel for a 1 s integration, expressed as a fraction of the counting rate from ε Gem. We denote this rms noise by $\epsilon(\phi)$ and compute it from several seconds of data before the occultation, when any variation in the data would be due to the noise only. If $n(t_j)$ is the mean counting rate for the jth integration bin of duration Δt (4 ms), N the number of integration bins, and $\bar{n}$ the average counting rate for all N integration bins, then

$$\epsilon(\phi) = \frac{(\Delta t)^{1/2}}{n_*}\left\{\frac{1}{N-1}\sum_{j=1}^{N}[n(t_j) - \bar{n}]^2\right\}^{1/2} . \qquad (1)$$

We consider two sources as likely causes of the rms noise level $\epsilon(\phi)$: photon noise (shot noise), and terrestrial scintillation. We believe that photon noise, and not scintillation noise, makes the dominant contribution for the following reason. The level of scintillation noise from Mars and ε Gem for a telescope at 12.5 km altitude predicted by equation (2.1.6) of Young (1974) yields $\epsilon(\phi) \approx 0.004$ for our channel 2, which is less than the value calculated from the

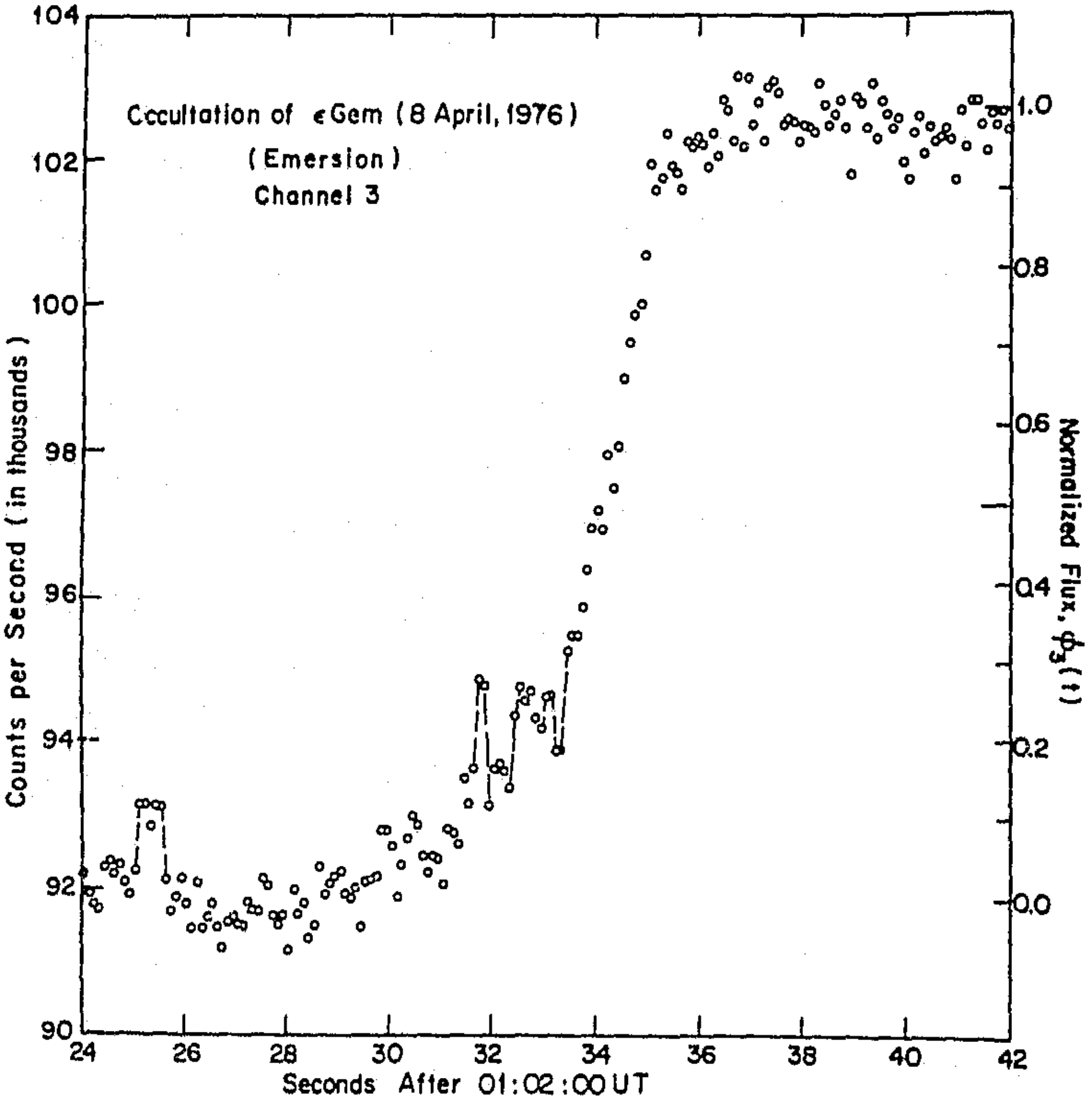

FIG. 3.—Emersion of ε Gem observed at 7500 Å; each point represents a 0.1 s integration. Prominent spikes are indicated by dashed lines.

observations (Table 1). Furthermore, the rms scintillation noise decreases exponentially with the altitude of the telescope above sea level. Hence Young's equation would also predict that a light curve for this occultation obtained from a ground-based telescope of similar aperture would have a rms noise level $\epsilon(\phi) = 0.02$ owing to scintillation alone. This would imply that the light curves obtained from ground-based telescopes would be about 3 times noisier than the airborne data, which appears to be confirmed (Wasserman, Millis, and Williamon 1977; Texas-Arizona Occultation Group 1977). Later, we hope to expand upon this necessarily brief discussion of noise encountered in airborne photometry.

III. TEMPERATURE, PRESSURE, AND NUMBER-DENSITY PROFILES

a) Method

When ε Gem was occulted by Mars, the process that caused the starlight to dim was differential refraction by the Martian atmosphere. From the light curves of Figures 2 and 3 we can obtain temperature, pressure, and number-density profiles for the Martian atmosphere if the following assumptions are satisfied: (i) the density gradients in the atmosphere are parallel to the local gravity gradient (i.e., perpendicular to the limb); (ii) the atmosphere is in hydrostatic equilibrium; and (iii) ray crossing is not severe (see § V of Elliot and

Veverka 1976). Under these assumptions we can obtain the desired profiles through the inversion technique of French, Elliot, and Gierasch (1977), which is similar to the "standard" inversion method (Kovalevsky and Link 1969; Hubbard *et al.* 1972; Wasserman and Veverka 1973), but has the advantage of assigning error bars to the temperature profiles. In the following discussion we use the notation for the occultation geometry shown in Figure 1 of French, Elliot, and Gierasch (1977).

From the observations we obtain the starlight intensity $\phi_\lambda(t)$ at a wavelength λ as a function of the time t. The intensity is normalized by the unocculted stellar intensity so that $\phi_\lambda(t)$ begins at 1.0 and drops to 0.0 for an immersion event. Invoking the assumptions of no ray crossing and no density gradients parallel to the limb, we can write an implicit equation for the time $t_\lambda(h - \Delta h)$ at which the asymptotic path of the starlight on the occultation curve has probed a level Δh deeper into the atmosphere at a previous time $t_\lambda(h)$:

$$\Delta h = v_\perp \int_{t_\lambda(h)}^{t_\lambda(h-\Delta h)} \phi_\lambda(t')dt' . \tag{2}$$

In equation (2), $v_\perp$ is the apparent velocity of the star perpendicular to the limb of Mars. For the same shell of atmosphere of thickness Δh, the refraction angle $\theta_\lambda(h)$ changes by $\Delta\theta_\lambda(h)$:

$$\Delta\theta_\lambda(h) = \frac{-v_\perp}{D} \int_{t_\lambda(h)}^{t_\lambda(h-\Delta h)} [1 - \phi_\lambda(t')]dt' , \tag{3}$$

where D is the Earth-Mars distance.

The function $\Delta\theta_\lambda(h)$ is the fundamental relation, obtained as a linear function of the occultation flux $\phi_\lambda(t)$, from which we can derive information about the Martian atmosphere. In addition to its dependence on refraction by the Martian atmosphere, $\phi_\lambda(t)$ contains noise that propagates into the values of Δh and $\Delta\theta_\lambda(h)$. If the noise that affects $\phi_\lambda(t)$ is Gaussian white noise (photon noise, for example), then $\sigma[\Delta h]$ and $\sigma[\Delta\theta_\lambda(h)]$, the rms errors for Δh and $\Delta\theta_\lambda(h)$, are given by

$$\sigma[\Delta h] = v_\perp\left[\int_{t(h)}^{t(h-\Delta h)} \sigma^2[\phi_\lambda(t')]dt'\right]^{1/2}$$

$$\sigma[\Delta\theta_\lambda(h)] = \frac{\sigma[\Delta h]}{D} , \tag{4}$$

where the integrand is the variance of $\phi_\lambda(t')$ for the time interval dt'.

We can write an equation for the number-density profile, $n(h)$:

$$n(h) = \frac{2\mathscr{L}}{\pi(2R_p)^{1/2}\nu_{\mathrm{STP}}(\lambda)} \int_h^\infty (h' - h)^{1/2} d\theta_\lambda(h') , \tag{5}$$

where $\mathscr{L}$ is Loschmidt's number, R_p is the radius of Mars, and $\nu_{\mathrm{STP}}(\lambda)$ is the refractivity of the atmosphere at STP. A similar integral can be given for the pressure profile $p(h)$ (French, Elliot, and Gierasch 1977):

$$p(h) = \frac{4g\bar{\mu}\mathscr{L}}{3\pi(2R_p)^{1/2}N_A\nu_{\mathrm{STP}}(\lambda)} \int_h^\infty (h' - h)^{3/2} d\theta_\lambda(h') , \tag{6}$$

where $\bar{\mu}$ is the (constant) mean molecular weight of the atmosphere, N_A is Avogadro's number, and g is the gravitational acceleration.

The atmospheric scale height $H(h)$ is defined by

$$H(h) = RT(h)/\bar{\mu}g , \tag{7}$$

where R is the universal gas constant and $T(h)$ is the temperature profile. To write equations (5) and (6), we have assumed $R_p \gg H(h)$. Combining equations (5)–(7) and the perfect gas law $p(h) = n(h)RT(h)/\bar{\mu}$, we can write an equation for the scale height that is independent of the atmospheric composition:

$$H(h) = \tfrac{2}{3} \int_h^\infty (h' - h)^{3/2} d\theta_\lambda(h') \Big/ \int_h^\infty (h' - h)^{1/2} d\theta_\lambda(h') . \tag{8}$$

Errors caused by the light curve noise enter into the values of $n(h)$, $p(h)$, and $H(h)$ through the integrands $d\theta_\lambda(h')$, and the magnitudes of the errors can be evaluated from the variances given by equation (4).

b) Application of the Method

To use the method outlined in the previous section we must first obtain the normalized occultation flux $\phi_\lambda(t)$. If t_j is the midtime of the jth 4 ms integration bin, then $\phi_\lambda(t_j)$ is given by

$$\phi_\lambda(t_j) = n(t_j) - [\alpha + \beta(t_j - t_0)]/n_* , \tag{9}$$

where $n(t_j)$ is the mean counting rate for the jth integration bin, n_* is the unocculted counting rate for ϵ Gem, t_0 is an arbitrary reference time, α is the background counting rate at time t_0, and β is the slope of the background counting rate. The value of $\phi_\lambda(t)$ for any time t is found by linear interpolation between the two appropriate values of $\phi_\lambda(t_j)$.

The constants n_*, α, and β were determined by a least-squares fit to an occultation curve appropriate for an isothermal atmosphere (Baum and Code 1953)[1] to each of our six light curves. The data interval used for each fit was 60 s, commencing 20 s before "half-light" for the immersion curves and covering the equivalent time interval for the emersion curves. In the fits, the counting rates α, β, and n_*, the scale height H, and the "half-light" time $t_{1/2}$, were free parameters. The background slope β was found to be comparable with its formal error in all cases and was therefore fixed at 0.0, while the other four parameters were varied. Values of α and n_* (with $\beta = 0.0$) obtained from these fits were used to obtain $\phi_\lambda(t)$ from equation (9).

[1] Although eq. (11) given by Baum and Code (1953) does not include the lateral focusing effects of a spherical planetary atmosphere, French *et al.* (1977) show that the resulting error introduced into the values of $n(h)$, $p(h)$, and $H(h)$ is negligible.

To evaluate the two fundamental integrals appearing in equations (5), (6), and (8), we have adopted the procedure of French, Elliot, and Gierasch (1977). First we obtained the $\Delta\theta(h)$ relation from the data by using equation (3) for equal Δh intervals of 1.0 km. Then two values of h were chosen: h_{max} [corresponding to $\phi_\lambda(t) \approx 0.99$] and h_0 [corresponding to $\phi_\lambda(t) \approx 0.7$]. The function $\Delta\theta(h) = (\theta_0/H)e^{-h/H}\Delta h$ (valid for an isothermal atmosphere of scale height H) was fitted by least squares to the values obtained from the data over the interval $h_0 \leq h \leq h_{max}$. The two free parameters in the fit were H and $\theta_0 H^{1/2}$, chosen to be independent. Our preference for this method over previous ones for establishing the boundary condition to begin the inversion calculation is explained in detail by French, Elliot, and Gierasch (1977).

The desired integrals were then evaluated in two parts. For $h_0 \leq h' < \infty$ the integrand was computed from the fitted $\Delta\theta(h)$ relation, and for $h \leq h' \leq h_0$ the integrand was computed from the $\Delta\theta(h)$ values obtained directly from the data. The errors in $n(h)$, $p(h)$, and $H(h)$ were computed with equations (21), (23), and (25) of French, Elliot, and Gierasch (1977).

Values used for the mean molecular weight $\bar{\mu}$ and the refractivity ν_{STP} are those for pure CO_2 gas (Old, Gentili, and Peck 1971). In addition to CO_2, the *Viking 1* lander found the atmosphere near the surface to contain 1%–2% argon and 2%–3% nitrogen (Owen and Biemann 1976). If the larger of these values applies to the atmosphere probed by the occultation events, then $\bar{\mu}$ and ν_{STP} for the Martian atmosphere are 1.3% and 1.8% less than the values for pure CO_2 gas. Hence our derived number densities will be 1.3% low, the temperatures 1.8% high, and the pressures 0.5% high.

c) *Results*

The number-density profiles obtained from equation (5) are shown in Figure 4 for the three immersion light curves and Figure 5 for the emersion light curves. The profiles have been dashed for altitudes greater than h_0

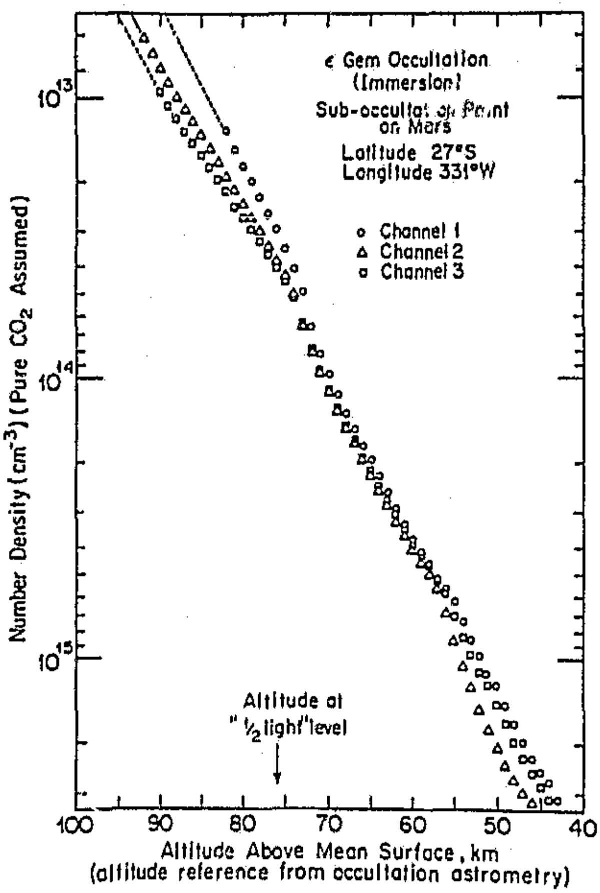

FIG. 4

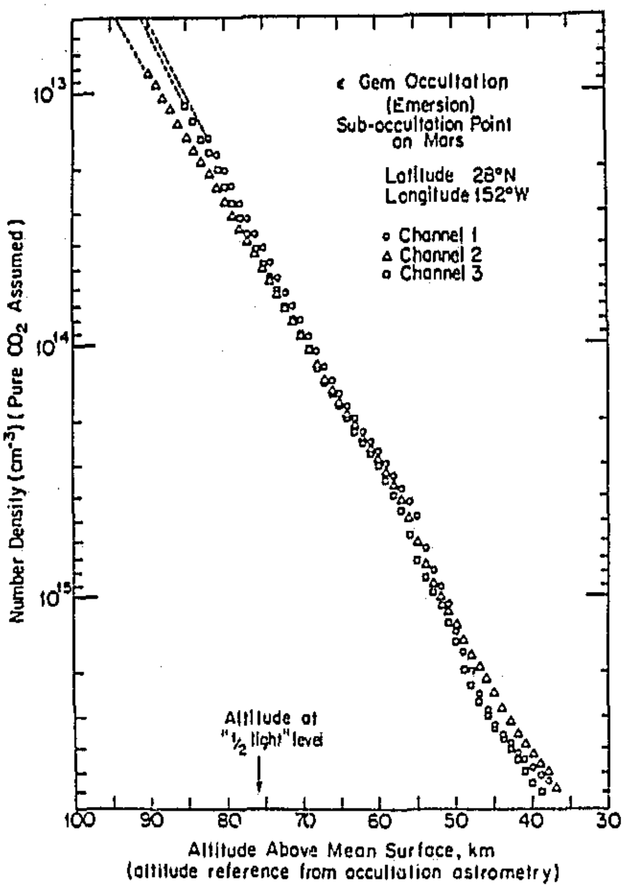

FIG. 5

FIGS. 4, 5.—Number-density profiles of the Martian atmosphere obtained by numerical inversion of the occultation light curve. The "half-light" altitude is estimated from occultation astrometry, and may be in error by several kilometers (see text). Internal and systematic errors are smallest in the region from 50 to 70 km. The dashed lines are computed from an isothermal fit to the initial data in each channel. As noted in the text, if the atmospheric composition measured by *Viking 1* lander (95% CO_2, 3% N_2, and 2% Ar; Owen and Biemann 1976) applies to the occultation level, the number densities shown here are 1.3% too low, the temperatures 1.8% too high, and the pressures 0.5% too high.

(region of the isothermal fit). The altitude scales for these and subsequent figures were obtained from a preliminary astrometric solution (Taylor 1976*b*).

The zero points for the immersion and emersion altitude scales are 3401 ± 5 km and 3404 ± 7 km from the center of Mars. From these values our altitude scales can be related to the altitude above the true surface for any model of the surface figure. The accuracy of the relative altitude scales for the same event but different channels depends on the integration of occultation light curve (eq. [2]); these should have errors of only 1–2 km. For clarity we have not plotted error bars on Figures 4 and 5, but the scatter of the values for the three different channels gives a good indication of the magnitude of the errors. Near the top of the profiles the errors are the largest. Then they decrease, reaching their minimum value (~3%) for number densities which correspond to an altitude of ~60 km before increasing again. The uncertainty in the baseline (α) of the occultation curve also causes an additional error in the profiles for low altitudes. We have ended our plots at levels where we believe the error caused by baseline uncertainty about equals the error caused by shot noise in the light curve.

Figures 6 and 7 show the pressure profiles for immersion and emersion obtained from equation (6). The behavior of the errors in these profiles is similar to that for the number-density profiles discussed above.

In Figures 8 and 9 we have plotted temperature versus number-density profiles for our light curves at 4500 Å; these had the lowest noise level (see Table 1). The shaded portion of the figure corresponds to altitudes greater than h_0, the region of the isothermal fit. The portions of the light curves required to generate these profiles are the segments shown in Figures 2 and 3. The error bars have been calculated from the light curve noise as described in the previous section. Since the noise that affects neighboring points in the profile is correlated, the random scatter of neighboring points is much less than the absolute error in temperature for each point (indicated by the error bars). The profiles show wavelike variations, with peak-to-peak amplitudes of ~35 K and a vertical scale of 20 km. These

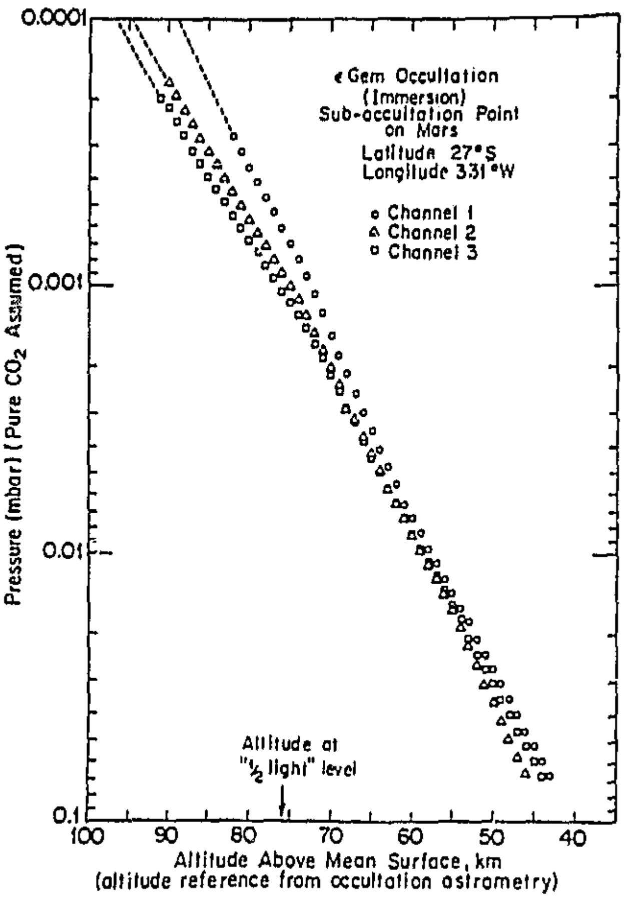

FIG. 6

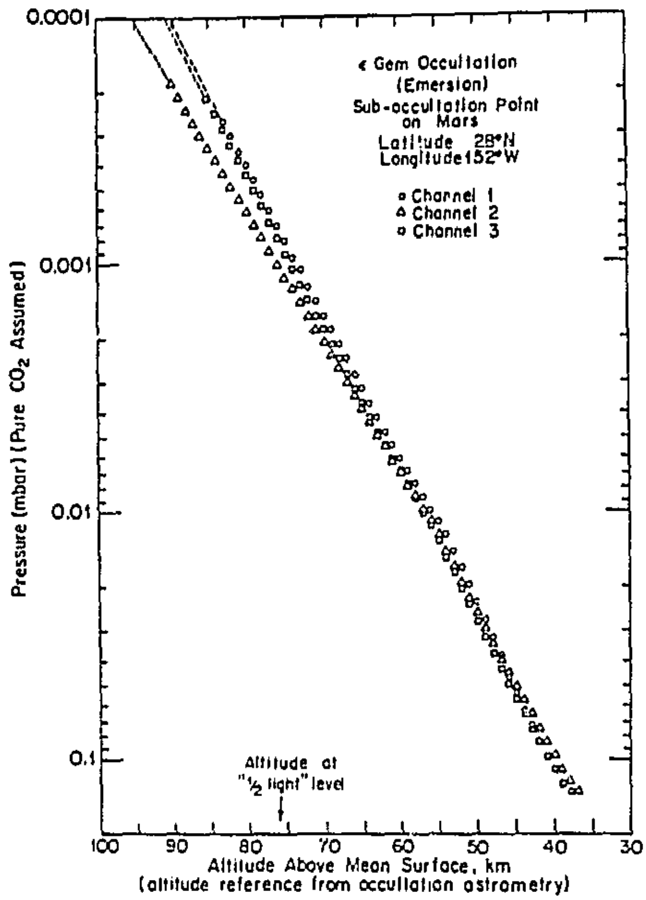

FIG. 7

FIGS. 6, 7.—Pressure profiles of the Martian atmosphere obtained by numerical inversion of the occultation light curve. The "half-light" altitude is estimated from occultation astrometry, and may be in error by several kilometers. Internal and systematic errors are smallest in the region from 50 to 70 km. The dashed lines are computed from an isothermal fit to the initial data for each channel.

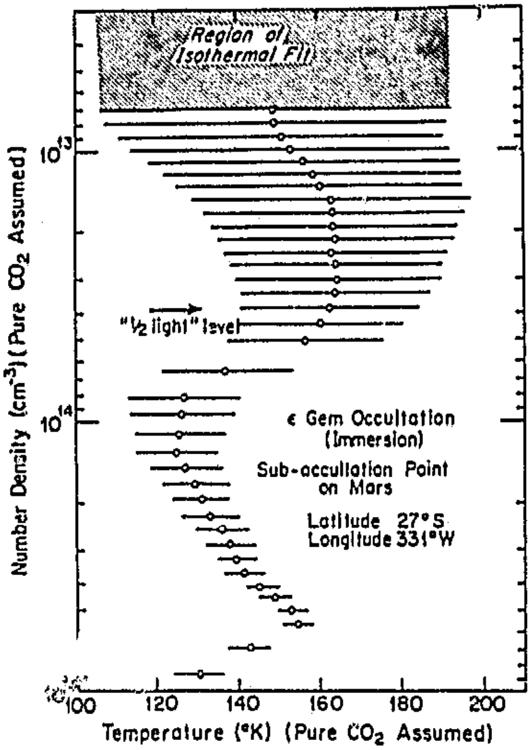

FIG. 8

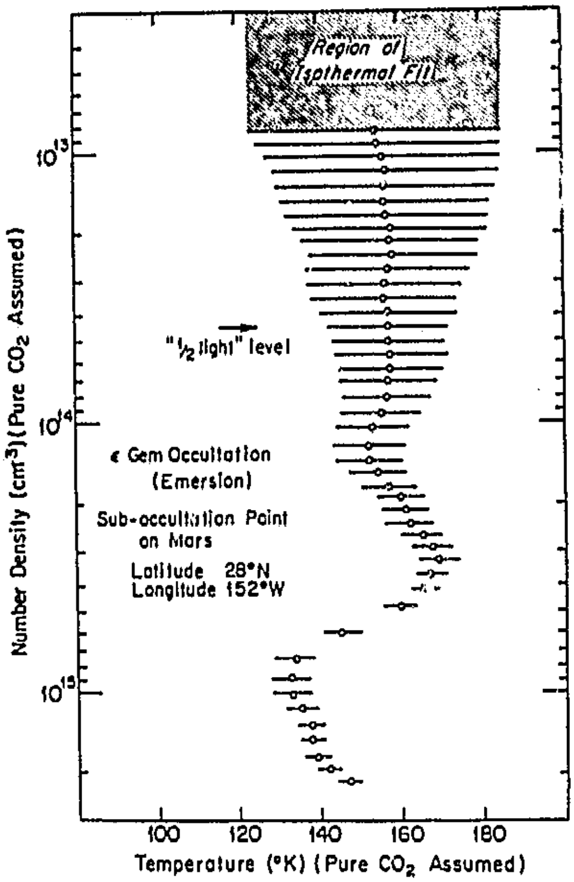

FIG. 9

FIGS. 8, 9.—Immersion and emersion temperature profiles obtained by numerical inversion of the channel 2 occultation light curve. The uncertainty in the isothermal fit to the initial data is shown dashed. The effects of random noise are shown by the error bars, which have a total length of two standard deviations. Because errors in successive points of the profile are highly correlated, short-scale temperature gradients are more reliable than implied by the error bars, which more properly reflect uncertainty in the positioning of the profile.

variations clearly exceed any that could be attributed to noise.

Temperature versus altitude profiles for all three channels are shown in Figures 10 and 11. The errors for each channel are proportional to the rms noise for that channel $\epsilon(\phi)$ (Table 1; French, Elliot, and Gierasch 1977), so that the error bars for channel 1 are about twice as large as those for channel 2 (see Figs. 7, 8); the errors for channel 3 are comparable with those for channel 2. The profiles mutually agree within their error bars.

The temperature *variations* on these profiles show better agreement than the absolute temperatures, because the variations are not sensitive to the large initial errors which affect the profile for several scale heights. Since the errors in successive points are correlated, short-scale temperature gradients are more reliable than implied by the error bars, which more properly reflect the uncertainty in the positioning of the profiles.

To see how well the short-scale temperature variations agree among the profiles for our three channels, we have removed a linear temperature fit from each profile. We write the temperature $T(h)$ in the following form:

$$T(h) = \left[\bar{T} + \overline{\frac{dT}{dh}}(h - \bar{h})\right] + \Delta T(h)\,, \qquad (10)$$

where $\bar{T}$ is the mean temperature and $\overline{dT/dh}$ is the mean temperature gradient over an altitude interval that has a mean altitude $\bar{h}$. The quantity $\Delta T(h)$ is the difference between $T(h)$ and the linear function in brackets (eq. [10]).

For each temperature profile we fit by least-squares for $\bar{T}$ and $\overline{dT/dh}$ over the altitude interval 55–80 km for the immersion profiles and 52–80 km for the emersion profiles. The (unweighted) average of the $\bar{T}$'s obtained from the three immersion profiles was 143 ± 11 K, and the average $\bar{T}$ for the emersion profiles was 146 ± 9 K. The mean temperature gradients obtained from the fits were $0.4 \pm 0.7\ \mathrm{K\ km^{-1}}$ and $-0.3 \pm 0.5\ \mathrm{K\ km^{-1}}$ for immersion and emersion. Clearly, these values depend on the altitude interval

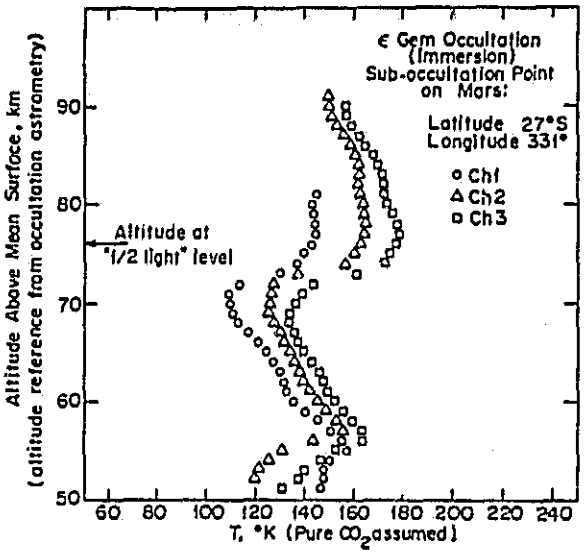

FIG. 10

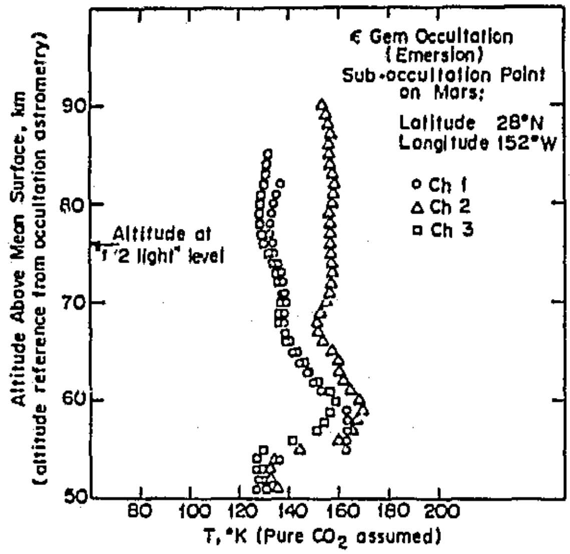

FIG. 11

FIGS. 10, 11.—Immersion and emersion temperature profiles obtained by numerical inversion of the occultation light curve. Internal and systematic errors are smallest between number densities of 2×10^{14} and 2×10^{15} cm^{-3}. Large-scale temperature variations with height are evident in all of the profiles. The largest temperature gradients are subadiabatic. The altitude corresponding to these measurements may be estimated from Figs. 4 and 5.

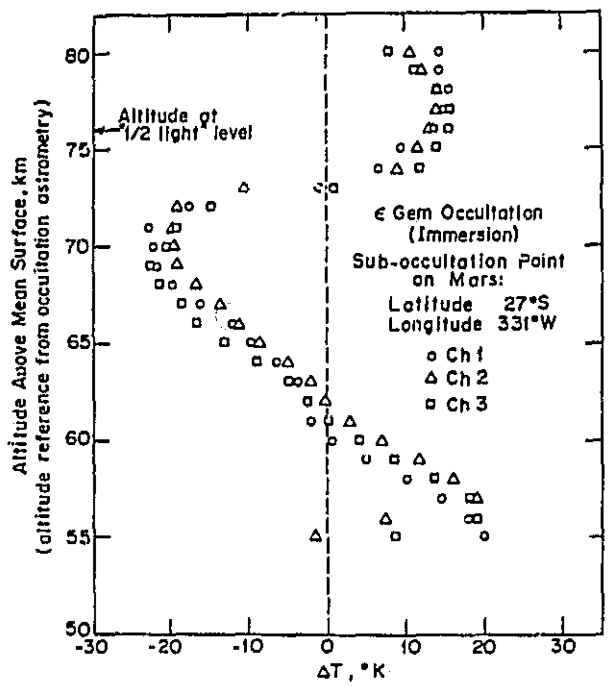

FIG. 12

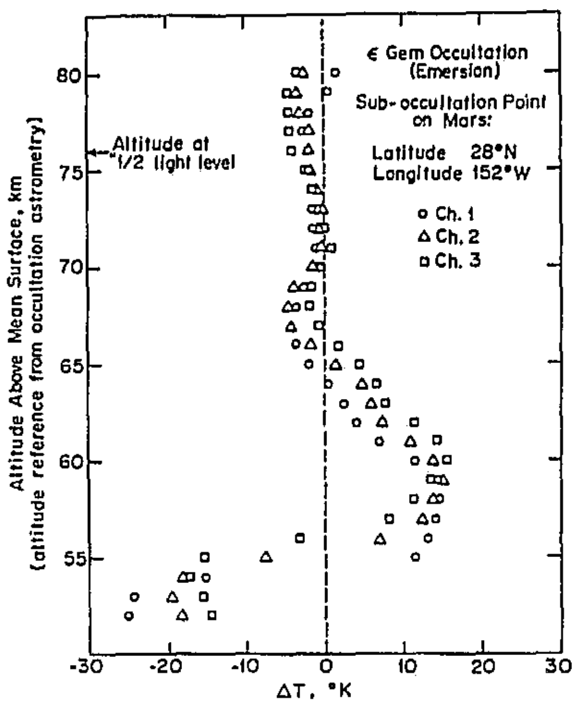

FIG. 13

FIGS. 12, 13.—Deviations of temperature profiles from a constant temperature gradient for immersion and emersion. For the altitude interval shown, a linear temperature gradient was fitted to the temperature profile obtained for each channel. ΔT is the deviation of the true profile from the fit at each point. The agreement among channels is excellent, with an average rms dispersion of 2–3 K, except near the end points. Pronounced wavelike structures are evident in both immersion and emersion profiles.

used for the fit—particularly its relation to the phase of the wavelike structures. Hence from this analysis we conclude only that our "mean" temperatures for immersion and emersion are not significantly different and that we see no large-scale gradients greater than ± 0.7 K km^{-1}.

After subtracting the linear fits from the temperature profiles, we have plotted the temperature residuals $\Delta T(h)$ in Figures 12 and 13. The agreement among the three profiles is excellent, with an average rms dispersion of 2–3 K except near the end points. The wavelike structures appear in both figures. The main difference among the profiles is the nearly isothermal character of the emersion profiles above about 70 km. We note that the immersion and emersion profiles are nearly identical in their region of overlap if the emersion profile is displaced 17 km upward. The altitude difference is significant, since the difference in the zero points of the immersion and emersion altitude scales should be not more than 12 km (see previous discussion). Further support for this conclusion is found from examination of Figures 8 and 9, where we see that a temperature maximum occurs at a number density of 6×10^{14} cm^{-3} for immersion; for emersion, however, the temperature maximum nearest to this occurs at a number density of 3.5×10^{14} cm^{-3}. This comparison is independent of the altitude scales and shows that the phase of the wavelike temperature variations, relative to the number density of the atmosphere, differs for the regions of the atmosphere probed by the immersion and emersion events.

We emphasize that other data and models can be compared directly with the profiles of Figures 12 and 13 only after a linear temperature fit is subtracted (eq. [10]).

IV. REFRACTIVITY DISPERSION AND ATMOSPHERIC COMPOSITION

From our light curves we can determine the ratio of the refractivity of the Martian atmosphere at two wavelengths, and from this measurement place limits on the amount of gases other than CO_2 in the atmosphere. The precision of this technique is inferior to that of the methods used by *Viking 1* (Nier *et al.* 1976; Owen and Biemann 1976), but is comparable with the precision of other remote sensing methods used to determine the helium fraction of Jupiter's atmosphere (Hunten and Veverka 1976). Hence a comparison of our results with the more accurate measurements of *Viking* is an important test of the occultation method for determining the composition of planetary atmospheres.

During the occultation, refractive dispersion of the gases that compose the Martian atmosphere caused the light curve $\phi_i(t)$ at wavelength λ_i to be delayed by a time τ relative to the light curve $\phi_j(t)$ obtained at wavelength λ_j, so that

$$\phi_i[t + \tau(t)] = \phi_j(t) . \tag{11}$$

The delay $\tau(t)$ is related to the refractivities of the atmosphere, ν_i and ν_j, at wavelengths λ_i and λ_j by the relation (derived from eqs. [6]–[9] of Elliot *et al.* 1974),

$$\tau(t) = \left(\frac{\nu_i}{\nu_j} - 1\right) \int_{-\infty}^{t} [1 - \phi_j(t')]dt' . \tag{12}$$

The refractivity ratio ν_i/ν_j for the atmosphere is the ratio of the sum of the refractivities of its constituent gases. If $f(\mathrm{Ar})$ and $f(CO_2)[=1 - f(\mathrm{Ar})]$ are the fractions by number of argon and CO_2 in a CO_2–argon atmosphere, then

$$\frac{\nu_i}{\nu_j} = \frac{f(CO_2)\nu(CO_2, \lambda_i) + f(\mathrm{Ar})\nu(\mathrm{Ar}, \lambda_i)}{f(CO_2)\nu(CO_2, \lambda_j) + f(\mathrm{Ar})\nu(\mathrm{Ar}, \lambda_j)} , \tag{13}$$

where the ν's are the refractivities of argon and CO_2 at wavelengths λ_i and λ_j. Fortunately, modern laboratory measurements of the refractivities of argon and CO_2 are available (Old, Gentili, and Peck 1971; Peck and Fisher 1964).

To use equation (13) we must also know the mean wavelengths of our three photometric channels, which are determined by combining the spectrum of ϵ Gem and the transmission profiles of the interference filters used. The mean wavelengths for channels 2 and 3 are nearly equal to the center wavelengths of the interference filters (Table 1), but the ultraviolet spectrum of ϵ Gem is steep, causing a significant and as yet undetermined shift of the mean wavelength of channel 1 to a larger value. Hence the light curve of channel 1 was not used in the present analysis.

For the Martian atmosphere, the refractivity ratio $\nu_3/\nu_2 - 1$ for $\lambda_2 = 4500$ Å, $\lambda_3 = 7500$ Å was determined by the following procedure. A portion of the light curve $\phi_2(t)$ (at 4500 Å) containing one or more spikes was selected for analysis, and for a test value of $\nu_3/\nu_2 - 1$, the time delays $\tau(t)$ were computed for each 4 ms integration bin with the aid of equation (12). The delays $\tau(t)$ were applied to the light curve $\phi_3(t)$ (at 7500 Å) to produce $\phi_3[t + \tau(t)]$. Then the sum of the squared differences, $\{\phi_2(t) - \phi_3[t + \tau(t)]\}^2$, was computed for 4 ms increments of t over the internal selected for analysis. The computation was carried out for test values of $\nu_3/\nu_2 - 1$ (in increments of 0.0005) within the range $-0.0300 \leq \nu_3/\nu_2 - 1 \leq -0.0100$. The test value that produced the minimum sum of squared differences was chosen as the best estimate of $\nu_3/\nu_2 - 1$ for that portion of the light curve.

The above procedure was applied to several regions of the immersion and emersion light curves that contained obvious spikes, and the resulting refractivity ratios are given in Table 2A. The error in their mean was computed from the internal consistency of the individual values. Next the procedure was applied to essentially the entire immersion light curve, from the beginning of the main intensity drop to the last major group of spikes, and to a corresponding interval of the emersion light curve. The refractivity ratios so obtained are given in Table 2B.

Since the two approaches to finding the refractivity are based on essentially the same data, we might expect somewhat better agreement between the two results. However, both are consistent with pure CO_2,

ORIGINAL PAGE IS
OF POOR QUALITY

TABLE 2

REFRACTIVITY RATIOS FOR THE MARTIAN ATMOSPHERE

A. Segments of Light Curves

Event	Beginning of Fitted Segment (s after 00:57:00 UT)	Length of Fitted Segment (s)	Refractivity Ratio $\{\nu(7500\ \text{Å})/\nu(4500\ \text{Å})\} - 1$
Immersion	20.0	8.6	−0.0208
Immersion	35.2	1.5	−0.0205
Immersion	51.0	0.8	−0.0225
Emersion	322.4	11.3	−0.0205
Emersion	315.4	1.2	−0.0185
		(Unweighted) Mean...	−0.0206 ± 0.0006

B. Major Portions of Light Curves

Event	Beginning of Fitted Segment (s after 00:57:00 UT)	Length of Fitted Segment (s)	Refractivity Ratio $\{\nu(7500\ \text{Å})/\nu(4500\ \text{Å})\} - 1$
Immersion	19.0	22.0	−0.0205
Emersion	315.0	20.7	−0.0225
		(Unweighted) Mean...	−0.0215 ± 0.0010

for which $\nu_3/\nu_2 - 1 = -0.0209$ (-0.0169 for pure argon). Version (B) of our analysis has the advantage of including all the data but probably has a greater error, since the spikeless portions of the curves contribute noise but no refractivity information. Hence we prefer version (A) of our analysis, since it presumably has a smaller error. This value (-0.0206 ± 0.0006) has been plotted in Figure 14, along with curves for the refractivity ratios for various gases. Our measurement corresponds to an argon fraction by number, f(Ar), equal to 10%(+20%, −10%). We note that this value applies to any combination of nitrogen and argon, since the refractivity ratios for these two gases are nearly equal (see Fig. 14). The amounts of argon and nitrogen found by *Viking* are 1%–2% and 2%–3% (Owen and Biemann 1976), consistent with our result.

V. ATMOSPHERIC EXTINCTION AND THE CENTRAL FLASH

The discovery of the central flash, the bright feature in the occultation light curve midway between immersion and emersion, presents an unexpected opportunity to determine an average for extinction in the Martian atmosphere at lower altitudes than probed by the immersion and emersion events. We shall show that the flash was formed through symmetric refraction by the Martian atmosphere when ε Gem was directly behind the center of Mars; our calculations show that this light passed through the atmosphere about 25 km above the mean surface. The integrated density along this slant path equals about 4 Martian air masses. The most abrupt variation in our observations of the central flash is the sharp rise at 00:59:56 UTC (Fig. 16), which has a duration $\Delta t \sim 0.5$ s; this establishes a minimum distance scale for large intensity variations within the Martian shadow of $v\Delta t \approx 10$ km. Since this is much greater than the Fresnel scale (0.2 km), we believe that a geometrical optics treatment is adequate for a preliminary analysis. From the optics and the astrometry, we estimate the mean optical depth of the atmosphere at the altitude sampled by the flash, and, by comparing the integrated flux of the central flash at different wavelengths, we determine the wavelength dependence of the atmospheric extinction.

a) *Intensity Profile of the Central Flash*

i) *Spherical Planet*

For an occultation by a spherical planet with an isothermal atmosphere, Baum and Code (1953) have derived an implicit equation for the occulted stellar intensity which is valid only near the limb of the planet's shadow (i.e., the immersion and emersion events). Hence to obtain an intensity profile for the central flash, we must write an equation for the stellar intensity that is valid throughout the shadow. To do this we use the derivation of Baum and Code (1953), with two additional effects included: (i) the curvature of the limb perpendicular to the line of sight, which causes the convergence of the light rays at the center of the shadow, producing the central flash; and (ii) the additional contribution of light from the "emersion limb." For a point a distance ρ from the center of the shadow, we define the "immersion limb" to be the point on the shadow limb closest to ρ and the "emersion limb" to be the most distant. We shall derive an equation for the normalized stellar intensity, $\phi(\rho)$; $\phi(t)$ can be obtained when $\rho(t)$ is specified.

If the atmosphere of the planet has a scale height H, then $\phi(\rho)$ is given by the equation derived by French (1977),

$$\phi(\rho) = 2H/\rho + \phi_+[1 - H/\rho] - \phi_-[1 + H/\rho] . \quad (14)$$

The functions ϕ_+ and ϕ_- are the intensities from the immersion and emersion limbs that would be obtained by neglecting the effects of limb curvature and are

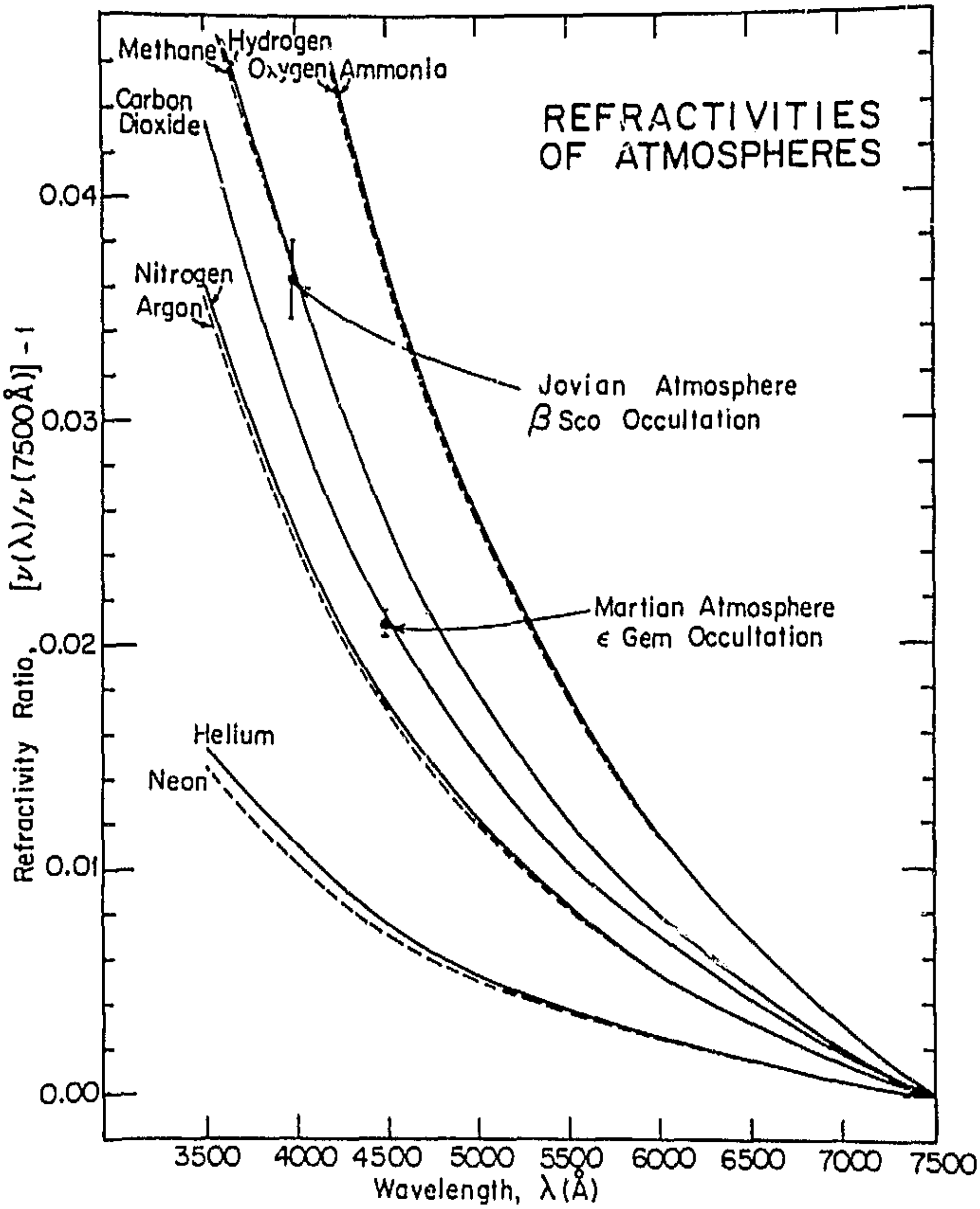

FIG. 14.—Refractivity ratio for the Martian atmosphere. The refractivity ratio $[\nu(\lambda)/\nu(7500\ \text{Å})] - 1$ for various gases is plotted, along with the value measured from the ϵ Gem occultation. The result indicates an atmosphere with 10%(+20%, −10%) argon and/or nitrogen, a value consistent with the composition found by *Viking 1* (Owen and Biemann 1976). The refractivity ratio determined for the Jovian atmosphere from the β Scorpii occultation (Elliot *et al.* 1974) has also been plotted. For purposes of comparison with the present result, the value of $[\nu(6201\ \text{Å})/\nu(3934\ \text{Å})] - 1$ actually measured for Jupiter has been scaled to $[\nu(3934\ \text{Å})/(7500\ \text{Å})] - 1$.

given implicitly by Baum and Code's equation (11):

$$\rho_0 - \rho = H\left[\left(\frac{1}{\phi_+} - 2\right) + \ln\left(\frac{1}{\phi_+} - 1\right)\right], \qquad (15)$$

$$\rho_0 + \rho = H\left[\left(\frac{1}{\phi_-} - 2\right) + \ln\left(\frac{1}{\phi_-} - 1\right)\right]. \qquad (16)$$

Here ρ_0 is the "half-light" radius of the shadow and is defined by $\rho_0 = \rho$ when $\phi_+ = \frac{1}{2}$.

Near the limb of the shadow, $\rho \gg H$ and $\phi_- \approx 0$. Making these approximations in equation (14), we find that $\phi(\rho) \approx \phi_+$, a result equivalent to Baum and Code's equation (11). Near the center of the shadow $\rho \approx H$ and $\phi_+ \approx \phi_- \ll 1$. From equation (14) we see that $\phi(\rho) \approx 2\ H/\rho$—the intensity of the central flash falls as ρ^{-1} away from its point of perfect geometrical focus in the center of the shadow.

The maximum intensity of the central flash is not infinite and will depend on the radius of the occulted star and diffraction, two effects not considered in the present model. If the stellar radius is the dominant effect and ρ_* is its projected radius at the distance of the planet from its shadow, then the maximum intensity at the center of the shadow is $4\,H/\rho_*$ for a uniformly bright stellar disk. The minimum intensity in the shadow occurs near $\rho = \rho_0/2$ and is approximately $16\,H/3\rho_0$. For the present occultation, this value is 0.016.

ii) *Oblate Planet*

Since Mars is significantly oblate, we have extended the model of the previous section to include this effect. The limb is assumed to be an ellipse, and consequently the radius of curvature varies from point to point along the limb. The locus of perfect focusing is no longer confined to the point $\rho = 0$, but forms a curve known as the evolute of the ellipse. To illustrate the situation, we refer to the ray optics diagram in Figure 15, where normals to the ellipse have been drawn at equal intervals along its perimeter; the evolute is seen as a concave diamond shape. However, the density of lines in Figure 15 is not a true indicator of the intensity throughout the shadow, since the decreasing intensity of each ray with increasing distance from the limb has not been illustrated.

If r_e and r_p are the equatorial and polar radii of the planet, the (x, y)-coordinates of the limb obey the equation for an ellipse,

$$\frac{x^2}{r_e^2} + \frac{y^2}{r_p^2} = 1\,, \tag{17}$$

and the (x, y)-coordinates of the corresponding evolute

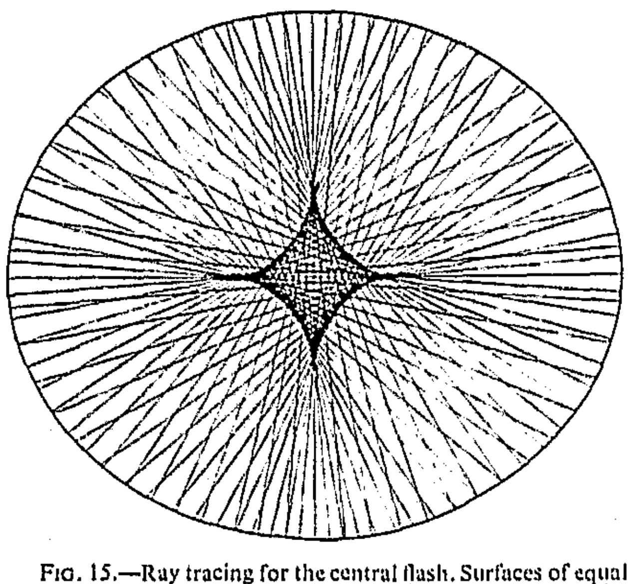

FIG. 15.—Ray tracing for the central flash. Surfaces of equal bending angle are assumed to be elliptical in shape. Density variations are assumed to be perpendicular to these surfaces, so that light is refracted along the normals to the ellipse. The intersections of these normals form a caustic curve—the evolute of the ellipse.

are obtained from the following implicit equation (Beyer and Selby 1976):

$$(r_e x)^{2/3} + (r_p y)^{2/3} = (r_e^2 - r_p^2)^{2/3}\,. \tag{18}$$

To calculate the intensity $\phi(x_0, y_0)$ for a point (x_0, y_0) within the shadow of an oblate planet, we used the following procedure. For each point (x_0, y_0) on the observer's path through the shadow, we find the points on the limb (x_l, y_l) whose normals intersect (x_0, y_0). After finding the distance d_l between (x_0, y_0) and (x_l, y_l), we calculate the intensity at (x_0, y_0) from Baum and Code's equation (11) for an atmosphere of scale height H. The intensity is then enhanced by the factor r_c/d, where r_c is the radius of curvature of the ellipse at (x_l, y_l) and d is the distance between (x_0, y_0) and the center of curvature of the ellipse at (x_l, y_l). Then the intensities from all points (x_l, y_l) on the limb whose normals intersect (x_0, y_0) are added to obtain $\phi(x_0, y_0)$. The procedure outlined involves exactly the same steps that were used to obtain the analytic solution $\phi(\rho)$ for a spherical planet (eq. [14]). Further details of the methods used for calculating $\phi(x_0, y_0)$ are given by French (1977).

In this model we have smoothed the central flash along the (x, y)-path (i.e., in one dimension only) by a triangular function that approximates the strip brightness distribution of ϵ Gem. If the atmosphere has a total optical depth τ through the path traversed by each ray, we can include this extinction effect by multiplying the entire profile by $e^{-\tau}$. Some of the light removed by extinction will in fact be scattered by the Martian atmosphere. Unless this scattering is strongly peaked at angles of a few arcsec (an unlikely possibility), this effect will not be important for our analysis.

b) Atmospheric Extinction

In the upper frame of Figure 16, we present light curves of the central flash at 0.1 s time resolution for all three wavelengths (Table 1). The values of the background intensity, α, and ϵ Gem intensity, n_*, used to obtain $\phi_\lambda(t)$ (eq. [9]) were the means of the values found for immersion and emersion. The lower frames of Figure 16 contain three model profiles of the central flash generated by the procedure described in the previous section. The path of the telescope relative to the evolute for each profile is shown in Figure 17. The shape of each profile was determined by five parameters: (i) $\epsilon = (r_e - r_p)/r_e$, the ellipticity of the model planet; (ii) ρ_m, the closest approach of the telescope path to the center of the planet; (iii) ψ, the angle between the telescope path and the shadow equator; (iv) H, the scale height of the model planet's atmosphere; and (v) τ, the optical depth of the atmosphere along the path traversed by the light rays, which is assumed to be the same for all rays. For all our model profiles we chose $H = 8$ km and varied τ to find the profile intensity scale that appeared to best fit the data.

For case A we adjusted all parameters except H to achieve the best agreement with the data. Note that

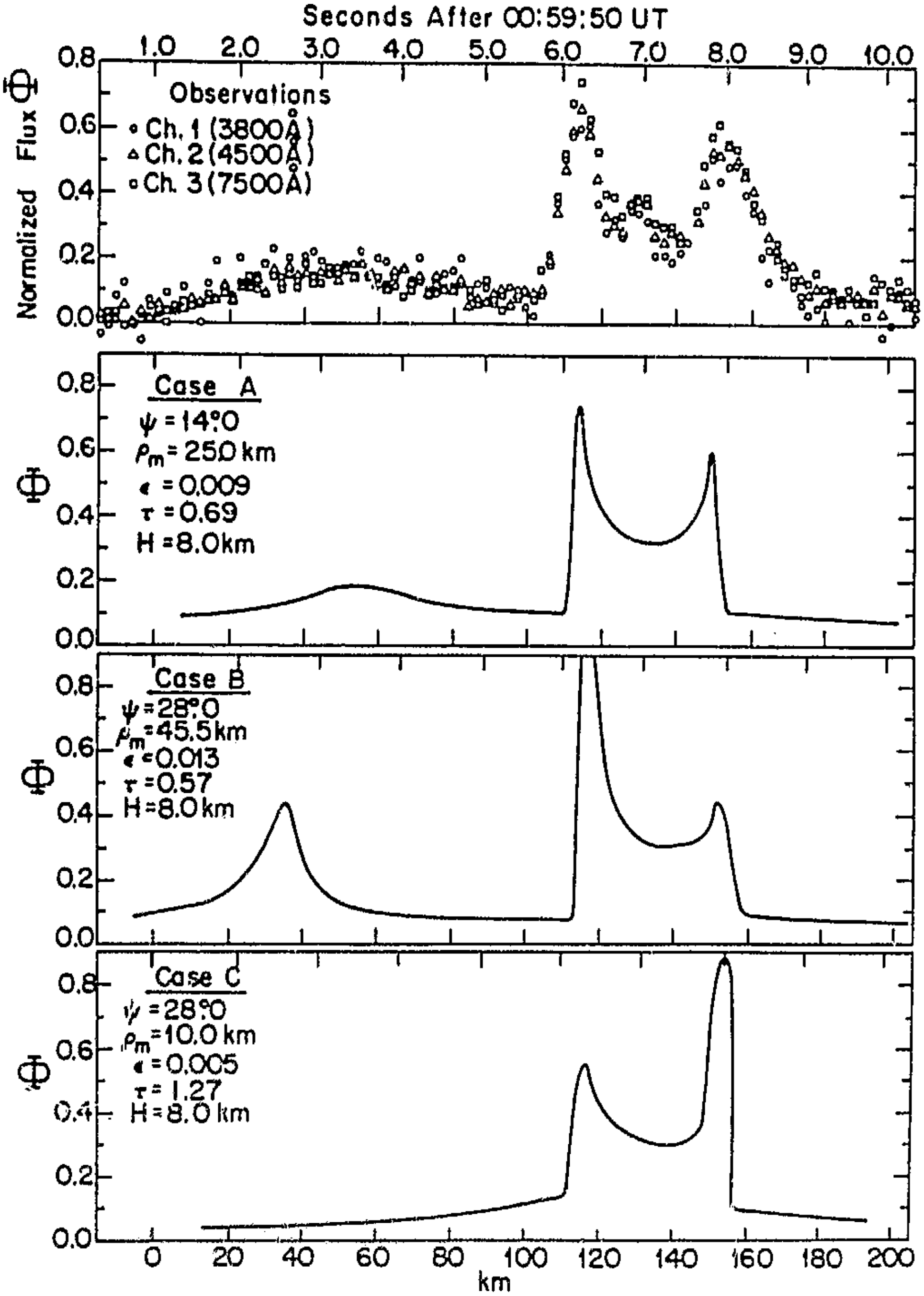

FIG. 16.—High time resolution data of the central flash and model central flash profiles. The relative areas under the profiles in the top frame provide information about the wavelength dependence of atmospheric extinction. Three model profiles are shown below, providing an estimate of the global atmospheric extinction along the slant path probed by the light which forms the central flash. The profiles have been smoothed by convolving with a uniformly bright stellar image with a radius of 3 km; ψ is the angle of the path of the telescope relative to the equator of the ellipse shown in Fig. 15, ρ_m is the closest approach of the path to the center of the ellipse, ϵ is the assumed oblateness of surfaces of equal bending angles, τ is the total optical depth through the atmosphere, and H is the scale height used in the calculation. The origin of the distance scale is arbitrary.

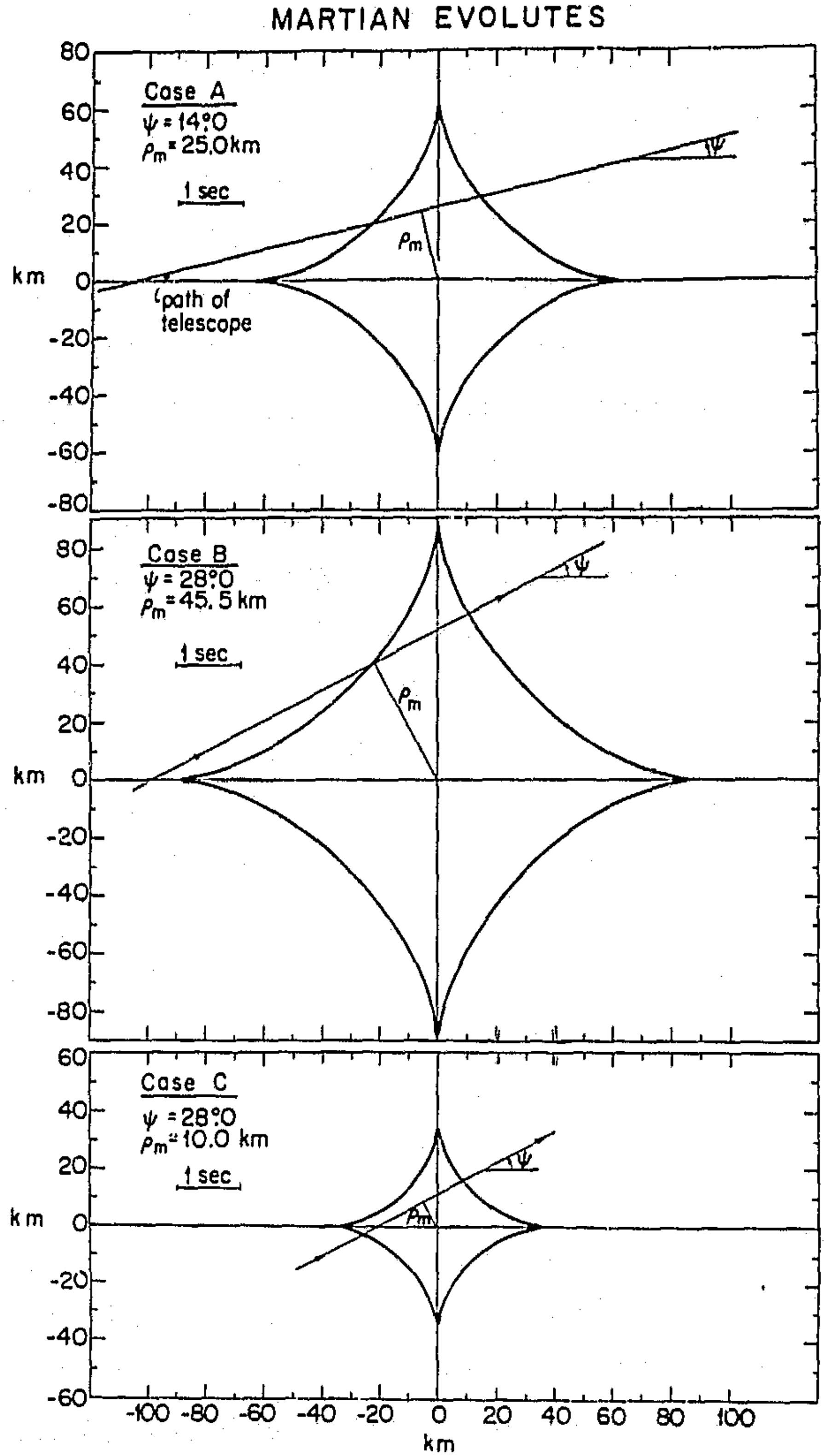

FIG. 17.—Martian evolutes, or loci of perfect focusing for rays refracted by an oblate planet with an isothermal atmosphere. The evolutes correspond to the concave diamond in the center of Fig. 15. The path of the telescope relative to the evolute is shown for each of the synthetic central flashes in Fig. 16. It is evident that the peaks in the synthetic profiles correspond to points nearest the evolute, where focusing is strongest.

the main features of the central flash can be reproduced: the broad wing at the left occurs when the path passes near a cusp of the evolute, and the two sharp peaks occur when the boundaries of the evolute are crossed.

For case B we set ψ and ϵ equal to the values indicated by the preliminary astrometric solution (Taylor 1976*b*), and adjusted ρ_m and τ for best agreement with the data. The last profile was obtained by fixing ψ at its value from the astrometric solution and fixing ϵ at 0.005, the ellipticity of the Martian surface (Christensen 1975). Again ρ_m and τ were varied to achieve the best fit to the data.

The values for ρ_m, ψ, and ϵ selected for the three model profiles would seem to bracket most reasonable possibilities, and these cases reproduce the main features of the data. Case A matches the data best, but the others use a more realistic value for ψ. We feel that the average optical depth τ along the path should lie somewhere between the extremes of cases A and C. For a definite value we chose the mean for these two cases, with error bars that include both extremes: $\tau = 0.90 \pm 0.45$. This is the total optical depth at 4500 Å along a slant path through the atmosphere sampled by the flash.

In order to relate this extinction to a definite column density of Martian atmosphere, we first write an equation for the number density $n(h_f)$ of the Martian atmosphere at the height h_f probed by the central flash,

$$n(h_f) = \frac{\mathscr{L} H^{1/2} \theta(h_f)}{\nu_{STP}(\lambda)[2\pi(R_p + h_c)]^{1/2}} \,. \tag{19}$$

We have assumed an isothermal atmosphere of scale height H, and the other quantities in equation (19) have been defined in § III. To evaluate equation (19), we note that at the center of the shadow the refraction angle of the light which forms the central flash is $\theta(h_f) = (R_p + h_c)/D$, and we make the approximation $h_f/R_p \ll 1$. For a CO_2 atmosphere, $\nu_{STP}(4500\ \text{Å}) = 4.55 \times 10^{-4}$, and letting $H = 8$ km, we find $n(h_f) = 1.75 \times 10^{16}\ \text{cm}^{-3}$. The main uncertainty in $n(h_f)$ is the scale height H, which must vary around the limb of the planet, for a $\pm 20\%$ variation in scale height $n(h_f)$ will be uncertain by $\pm 10\%$.

The column density $N(h_f)$ of atmosphere traversed by the light that forms the central flash is given by

$$N(h_f) = \frac{n(h_f)[2\pi(R_p + h_f)H]^{1/2}}{\mathscr{L}} = \frac{HR_p}{D\nu_{STP}(\lambda)} \,. \tag{20}$$

From equation (20) we find $N(h_f) = 0.27$ km atm[2] where again the main uncertainty enters through the scale height H. This value of $N(h_f)$ is equivalent to about 4 Martian air masses if we assume one Martian air mass to be 0.070 km atm (Young 1969). Hence the optical depth of 0.90 ± 0.45 is about 3.3 ± 1.7 per km atm, or about 0.23 ± 0.12 per Martian air mass.

[2] One km atm (kilometer atmosphere) is the thickness of the gas column in kilometers when compressed to standard temperature and pressure (i.e., 2.687×10^{24} molecules per cm^2).

Finally, we write an equation for the altitude of the atmosphere probed by the central flash:

$$h_f = H \ln\left[\frac{n(0)}{n(h_f)}\right] , \tag{21}$$

where $n(0)$ is the number density at the mean surface and $\bar{H}$ is an average scale height between the surface and h_f. For $\bar{H} = 10$ km and a surface number density of $2.1 \times 10^{17}\ \text{cm}^{-3}$, we find $h_f = 25$ km. For different values of $n(0)$ and $\bar{H}$ that occur around the planet, h_f would lie in the range 20–30 km.

c) Wavelength Dependence of the Extinction

We can also determine the wavelength dependence of the optical depth by comparing the light curves of the central flash at different wavelengths. If $\tau(\lambda_i)$ is the optical depth of the Martian atmosphere for the ith channel (Table 1) and $\phi_i(t)$ is the normalized flux for that channel (eq. [9]), then the following equation holds:

$$\phi_1(t) \exp[+\tau(\lambda_1)f(\lambda_1)] = \phi_2(t) \exp[+\tau(\lambda_2)f(\lambda_2)] = \phi_3(t) \exp[+\tau(\lambda_3)f(\lambda_3)] \,, \tag{22}$$

where $f(\lambda)$ is a function that accounts for the fact that each wavelength samples a slightly different altitude because of the variation of refractivity with wavelength (§ IV). For these calculations we let $f(\lambda) = 1$. We adjusted the value of the optical depth difference, $\tau(\lambda_1) - \tau(\lambda_2)$, to minimize the squared difference between $\phi_1(t)$ and $\phi_2(t)$ within the time interval containing the central flash (from 00:59:46.9 to 01:00:02.9 UTC; see Fig. 16) and obtained the value $\tau(3800\ \text{Å}) - \tau(4500\ \text{Å}) = 0.06 \pm 0.03$. The same procedure applied to $\phi_2(t)$ and $\phi_3(t)$ yielded the optical depth difference $\tau(4500\ \text{Å}) - \tau(7500\ \text{Å}) = 0.13 \pm 0.02$.

We have plotted these results in Figure 18, where we see that the relative extinction at different wavelengths is determined much better than the absolute value. The wavelength dependence of the optical depth is weaker than calculated for Rayleigh scattering, and the lower bounds on the optical depths greatly exceed the Rayleigh scattering value. We conclude that other extinction processes—by haze, dust, or high-level water-vapor clouds—were dominant at the 25 km level of the Martian atmosphere at the time of our observations.

Although our model explains several features of the central flash, the best model profile does not fit the data within the uncertainties of the random noise on the light curves. To extend this analysis, values of ρ_m and ψ can be fixed when the final astrometric solution is available and the isothermal assumption can be replaced by a more realistic representation of horizontal and vertical temperature gradients. Also, since each segment of the central flash originates from a different region of the limb, it may be possible to obtain regional, rather than global, extinction information. The present astrometric solution (Taylor

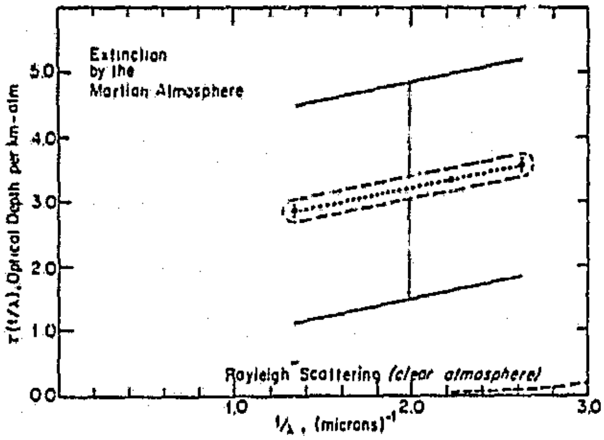

FIG. 18.—Extinction by the Martian atmosphere as a function of wavelength, determined from the central flash. The central flash probes the atmosphere along a slant path whose closest approach to the Martian surface is at an altitude of 25 km. This corresponds to a column density of about 4 Martian atmospheres. The large error bar represents the uncertainty in the absolute optical depth, estimated by comparing synthetic central flash profiles to the data. The small error bars show the uncertainty in the *relative* extinction from channel to channel, determined from relative fluxes of the central flash in each channel.

1976*b*) indicates that the airborne telescope passed north of the shadow center. For this path the preceding broad shoulder of the central flash was formed by light passing near the Martian equator (near 150° W longitude), while the light in the two larger peaks passed over the south polar region.

VI. DISCUSSION

The ϵ Gem occultation occurred just 15 weeks before *Viking 1* entry experiments, which measured the structure of the Martian atmosphere within the same altitude range probed by the occultation. Before *Viking 1* landed on Mars, the results of § IV and some of the results of §§ III and V were issued in a report (Elliot *et al.* 1976*b*). These results served to assure the *Viking* Project that the entry dynamics had been configured for a proper model Martian atmosphere. The number densities probed by the occultation event correspond to the critical level for the aerodynamic braking of an entry probe.

Now for the first time we can compare temperature profiles obtained from a stellar occultation with in situ measurements. The preliminary *Viking 1* temperature profile (Nier *et al.* 1976) shows a mean temperature of ~ 130 K, slightly cooler than our values (~ 145 K), in the altitude range 50–80 km. Wavelike temperature structures, with a vertical scale of 20 km, appear on both our immersion and emersion profiles as well as the *Viking 1* temperature profile. The pressure profiles from the occultation are comparable to that of *Viking 1* (see Fig. 5 of Nier *et al.* 1976). As mentioned in § IV, the composition inferred from our measurement of the refractivity ratio agrees within its error to the composition determined by *Viking*. Our values of the extinction are comparable with those found by the *Viking* landers (Mutch *et al.* 1976*a*, *b*, *c*; Pollack 1976), but the *Viking* results on the wavelength dependence of the extinction are not yet available for comparison.

Since different regions of atmosphere were probed at different times by the occultation and *Viking 1*, we would not expect precise agreement of the temperature profiles. More detailed comparison should be done on the basis of a model that describes the time and space behavior of the temperature of the upper atmosphere. But it is clear that the agreement of the mean temperatures and the qualitative features of the wavelike structures are significant evidence for the validity of both procedures.

In the context of the β Scorpii occultation Elliot and Veverka (1976) discuss the validity of two important assumptions used to obtain our present results—that ray crossing is not severe and that the density gradients are parallel to local gravity. For Jupiter they concluded that (i) at least some atmospheric structures that cause the spikes extend several km along the limb; and (ii) there is no compelling evidence to prove that the spike-producing structures either do or do not extend for several thousand km. Young (1976) proposed that the spikes and other irregularities in occultation light curves are caused by atmospheric turbulence, which must necessarily be anisotropic to explain certain features of the β Scorpii data. If Young's proposal is correct, the details of the temperature inversions obtained from the β Scorpii data would be indicative of turbulence, but not of any large-scale atmospheric structures. However, other quantities derived from the data on the basis of the gravity-gradient model (i.e., the [He]/[H_2] ratio and the diameters and separation of β Scorpii A_1 and A_2) would be essentially the same as would be obtained from an anisotropic turbulence model. On the basis of the same data, Jokipii and Hubbard (1977) argue for an isotropic turbulence model, which would discount all quantities derived from the β Scorpii data except for the mean temperature of the atmosphere obtained from isothermal fits. The McDonald Observatory observations of the ϵ Gem occultation have been analyzed in terms of the isotropic turbulence model by the Texas-Arizona Occultation Group (1977), who find a mean temperature of 190 ± 50 K—a mean value and probable error substantially greater than our results and the *Viking 1* results.

We now consider what region of the atmosphere must have no horizontal refractivity gradients for our assumption to be satisfied for the purposes of inversion of the ϵ Gem data. As illustrated for the β Scorpii occultation by Jupiter in Figure 12 of Elliot and Veverka (1976), we see that at any given time the atmosphere causing 67% of the refraction is in the shape of a "squashed cylinder" (refraction cylinder) with its long axis along the line of sight. For the ϵ Gem occultation, the length of the cylinder is $2(R_pH)^{1/2} \approx$ 300 km, and its diameter about 6 km (the projected diameter of ϵ Gem at Mars) when the occultation begins. The axis of the cylinder perpendicular to the limb decreases by the factor ϕ (normalized occultation flux) as the occultation proceeds. Since the airborne telescope was arranged to be on the center line, the motion of the refraction cylinder parallel to the limb was only a few km. The refraction cylinder extended almost exactly along a parallel of Martian latitude, and its length was about 6° of longitude.

Large-amplitude waves with long horizontal and vertical wavelengths satisfy all the assumptions of the spherical shell model used to invert the light curves. Large amplitudes allow identification of the waves in the presence of random noise. Long horizontal wavelength implies that a given shell maintains its character over the entire path of integration, and long vertical wavelengths mean that the wave is associated with broad features in the light curve, and does not depend on detailed structure of a sharp spike.

One method of checking for horizontal refractivity gradients along longitudes is to compare the light curves and temperature profiles with other ϵ Gem occultation observations of sufficiently high signal-to-noise ratio (Wasserman, Millis, and Williamon 1977). This work is in progress.

Another check on our assumptions is to compare the direct measurements of atmospheric composition made by *Viking 1*. Within the errors of the present occultation measurement, the occultation result (see Fig. 14 and § IV) agrees with the composition found by *Viking*. Hence we must conclude either that the method is insensitive to horizontal refractivity gradients (turbulence, for an example) or that the Martian atmosphere has small horizontal refractivity gradients.

VII. CONCLUSIONS

The Martian atmosphere probed by our occultation observations has temperatures within the range ~130–170 K for altitudes between 50 and 90 km above the mean surface. The wavelike structure of the temperature variations on a vertical scale of 20 km may be due to tides (Elliot *et al.* 1976*a*) or may represent the equilibrium atmospheric structure—perhaps arising from photochemical processes. The atmosphere extinction (at an altitude of 25 km) has a wavelength dependence too weak and a magnitude too large to be explained entirely by Rayleigh scattering.

The mean temperature, its wavelike structure, and the atmospheric composition inferred by our differential refractivity measurement agree with in situ measurements made by *Viking 1*. We feel that this agreement strongly supports the use of occultations as reliable and inexpensive probes of planetary upper atmospheres. The technique seems particularly sensitive to variations in temperature that have a large horizontal scale but a vertical scale of 2 scale heights or less. Only the events of intrinsically high signal-to-noise ratio are potentially useful, and to obtain good temperature profiles and other information from these relatively rare events, light curves with low noise and stable baselines are essential.

In this regard, airborne observations offer the advantages of telescope mobility, reduced scintillation noise, and operation above possible clouds. For this particular occultation our temperatures, pressures, number densities, and differential refractivity measurement would have been at least 3 times noisier (due to scintillation), and the extinction information of the central flash would not have been obtained, had we observed from the ground—even using a large telescope.

We are extremely grateful to R. Cameron, C. Gillespie, J. McClenahan, and the rest of the staff of the Kuiper Airborne Observatory for their advice, cooperation, and able assistance. The central flash would not have been discovered without G. E. Taylor's reliable predictions, based on an accurate Martian ephemeris from JPL, and the skill of navigator Bob Morrison and pilot Ron Gerdes. We thank A. T. Young, R. Zurek, R. Millis, L. H. Wasserman, and W. B. Hubbard for helpful discussions, and J. Goguen, M. Roth, and S. Arden for help in preparing for our observations. We appreciate the interest in this project of D. M. Hunten, W. A. Baum, J. B. Pollack, and C. B. Leovy, and thank S. I. Rasool and N. W. Boggess for their encouragement. The observations would not have been possible without the rapid consideration of our proposal by R. F. Fellows, which resulted in NASA grant NSG 7243 to support this work. Partial support was also provided by NASA grants NGR 33-010-082, NGR 33-010-186, NSG 2174, and NSG 7126, and NSF grant MPS 75-06670. Peter J. Gierasch is supported in part by an Alfred P. Sloan Research Fellowship.

REFERENCES

Baum, W. A., and Code, A. D. 1953, *A.J.*, 58, 108.
Beyer, W. H., and Selby, S. M. 1976, *Standard Mathematical Tables* (24th ed.; Cleveland: CRC Press), p. 319.
Christensen, E. J. 1975, *J. Geophys. Res.*, 80, 2909.
de Vegt, C. 1976, *Astr. Ap.*, 47, 457.
Dunham, E., and Elliot, J. L. 1977, in preparation.
Elliot, J. L., Dunham, E., and Church, C. 1976, *Sky Tel.*, 52, 23.
Elliot, J. L., French, R. G., Dunham, E., Gierasch, P. J., Veverka, J., Church, C., and Sagan, Carl. 1976*a*, *Science*, 195, 485.
Elliot, J. L., French, R. G., Dunham, E., Gierasch, P. J., Veverka, J., Sagan, C., and Church, C. 1976*b*, report prepared for *Viking* Project use, June.
Elliot, J. L., and Veverka, J. 1976, *Icarus*, 27, 359.
Elliot, J. L., Veverka, J., and Goguen, J. 1975, *Icarus*, 26, 387.
Elliot, J. L., Wasserman, L. H., Veverka, J., Sagan, Carl, and Liller, W. 1974, *Ap. J.*, 190, 719.
French, R. G. 1977, Ph.D. thesis, Cornell University.
French, R. G., Elliot, J. L., and Gierasch, P. J. 1977, *Icarus*, in press.
Hubbard, W. B., Nather, R. E., Evans, D. S., Tull, R. G., Wells, D. C., Van Citters, G. W., Warner, B., and Vanden Bout, P. 1972, *A.J.*, 77, 41.
Hunten, D. M., and Veverka, J. 1976, in *Jupiter*, ed. T. Gehrels (Tucson: University of Arizona Press), p. 247.
Jokipii, J. R., and Hubbard, W. B. 1977, *Icarus*, 30, 537.
Kovalevsky, J., and Link, F. 1969, *Astr. Ap.*, 2, 398.
Mutch, T. A., *et al.* 1976*a*, *Science*, 193, 791.
———. 1976*b*, *Science*, 194, 87.

Mutch, T. A., *et al.* 1976*c*, *Science*, 194, 1277.
Nier, A. O., Hanson, W. B., Seiff, A., McElroy, M. B., Spencer, N. W., Duckett, R. J., Knight, T. C. D., and Cook, W. S. 1976, *Science*, 193, 786.
Old, J. G., Gentili, K. L., and Peck, E. R. 1971, *Opt. Soc. Am.*, 61, 89.
Owen, G. T., and Biemann, K. 1976, *Science*, 193, 801.
Peck, E. R., and Fisher, D. J. 1964, *J. Opt. Soc. Am.*, 54, 1362.
Pollack, J. B. 1976, private communication.
Taylor, G. E. 1976*a*, personal communication.
Taylor, G. E. 1976*b*, *Nature*, 264, 160.
Texas-Arizona Occultation Group. 1977, *Ap. J.*, 214, 934.
Wasserman, L. H., Millis, R. L., and Williamon, R. M. 1977, *A.J.*, in press.
Wasserman, L. H., and Veverka, J. 1973, *Icarus*, 20, 322.
Young, A. T. 1974, in *Methods of Experimental Physics: Astrophysics*, ed. N. Carleton (New York: Academic Press), p. 95.
———. 1976, *Icarus*, 21, 335.
Young, L. D. G. 1969, *Icarus*, 11, 386.

C. Church, E. Dunham, J. L. Elliot, R. G. French, P. J. Gierasch, Carl Sagan, and J. Veverka: Laboratory for Planetary Studies, Cornell University, Center for Radiophysics and Space Research, Ithaca, NY 14853

A Unique Airborne Observation

J. L. Elliot, E. Dunham, and C. Church

Laboratory for Planetary Studies

Cornell University

Reprinted from Sky and Telescope, Vol. 52, No. 1, *July, 1976.*

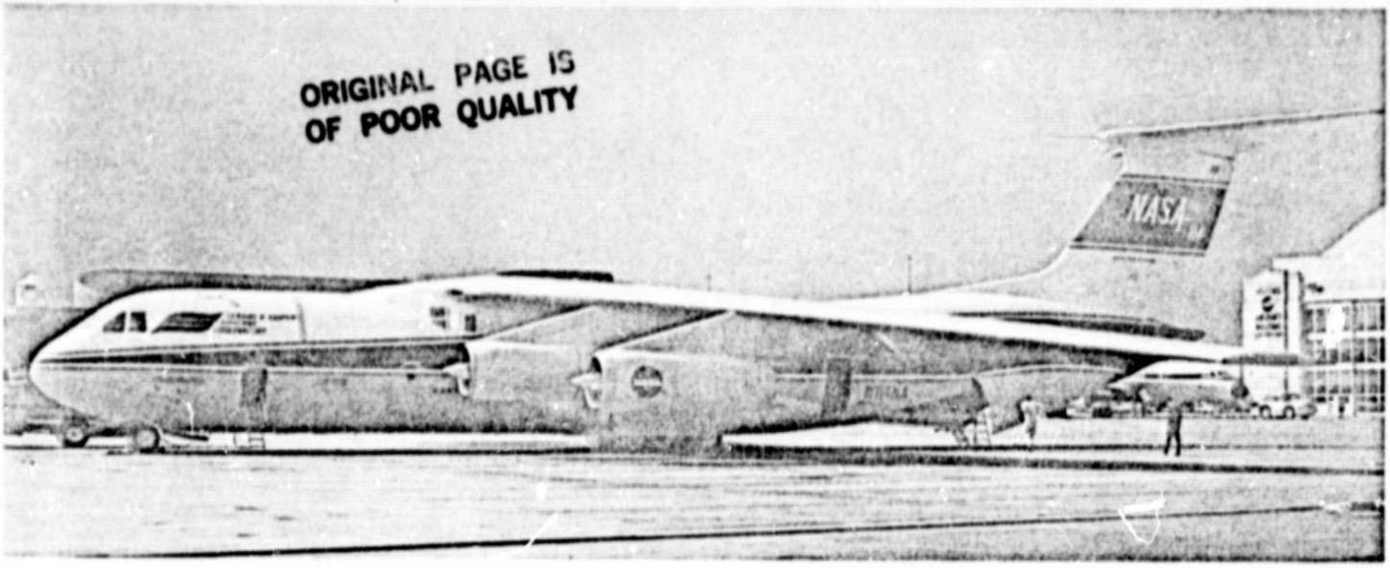

The observations described in this article were made aboard the Kuiper Airborne Observatory, seen here at its base, Moffett Field, California. This C-141 jet is named after G. P. Kuiper, who pioneered in infrared astronomy from aircraft.

A Unique Airborne Observation

J. L. ELLIOT, E. DUNHAM, and C. CHURCH, *Laboratory for Planetary Studies, Cornell University*

THE OCCULTATION of 3rd-magnitude Epsilon Geminorum by Mars on April 8th gave us a rare opportunity to probe directly the refractive properties of the Martian atmosphere. Unlike a lunar occultation, during which starlight is cut off abruptly by the moon's limb, the light from Epsilon Geminorum was dimmed gradually by differential atmospheric refraction — the same phenomenon that causes the oblate appearance of the sun near the horizon. From our observations we will obtain information about the temperature structure and composition of Mars' atmosphere; similar measurements are planned for the Viking lander this month.

Along with our colleagues Joe Veverka and Carl Sagan, we wanted to learn as much as possible about the Martian atmosphere. Hence, we had to obtain photoelectric light curves with a minimum of background noise. This presented a problem, since from North America the occultation was visible in darkness only in the East, where generally poor observing conditions prevail in the spring. Even if the skies were clear (as they proved to be at most sites, see the last page), scintillation in the earth's atmosphere would seriously degrade the photometry. Also, no moderate-sized telescope was situated near the center line of the occultation, the ideal location for our observations.

The solution to these problems proved to be NASA's Gerard P. Kuiper Airborne Observatory (KAO). Dedicated in May, 1975, this C-141 aircraft contains a 36-inch telescope that is used for infrared observations, above most of the water-vapor absorption in the earth's atmosphere. The capability of observing from altitudes as high as 45,000 feet — well above clouds and most scintillation — seemed to make KAO ideal for occultation work.

However, since neither optical photometry nor occultation observations had been tried from the KAO, many people were skeptical that high-quality data could be obtained. It was feared that the boundary layer of air rushing past the telescope port, among other factors special to the aircraft, would make the light curve noisier than if obtained from the ground. The best way to resolve the question was to observe the occultation!

In early March our request to use the

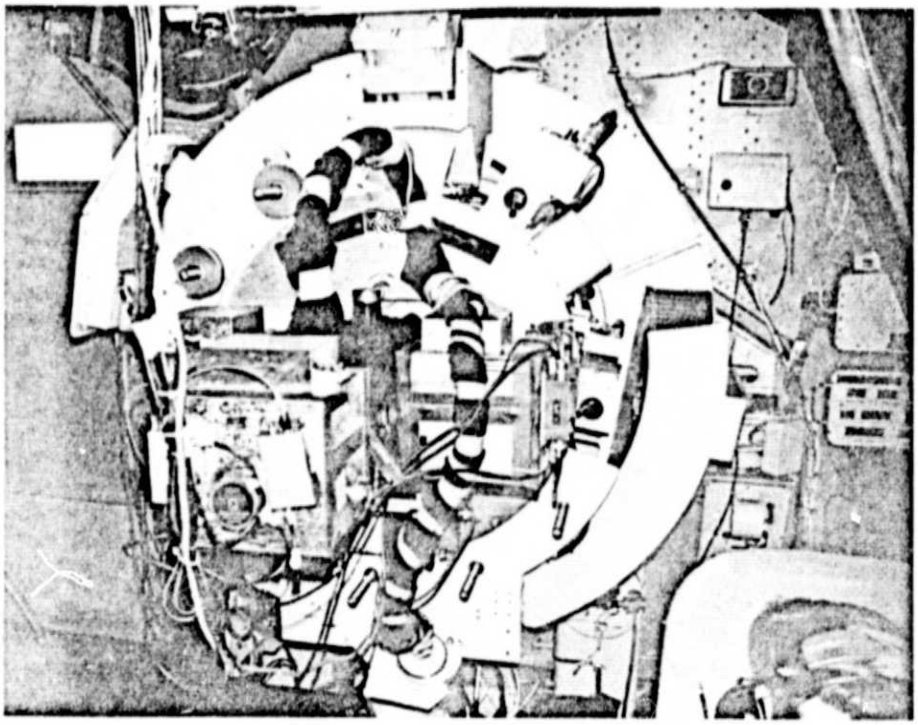

In this view inside the KAO, the photoelectric photometer employed for the occultation is mounted at the bent Cassegrain focus of the 36-inch telescope. Except as noted, all illustrations are from the authors.

This work was supported by NASA grant NSG-7243 and other NSF and NASA grants.

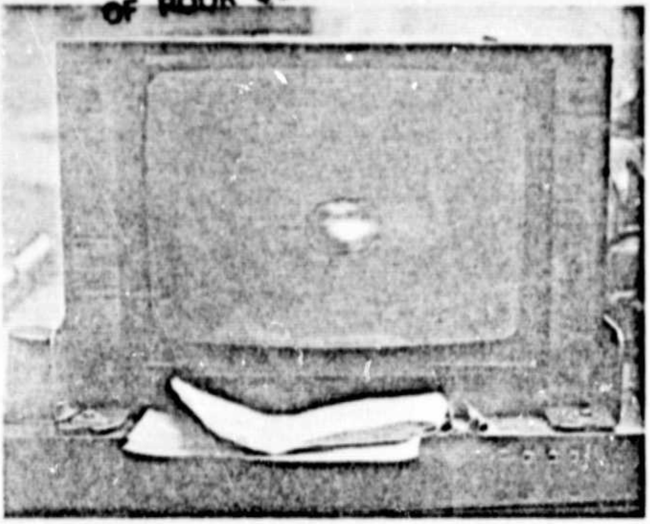

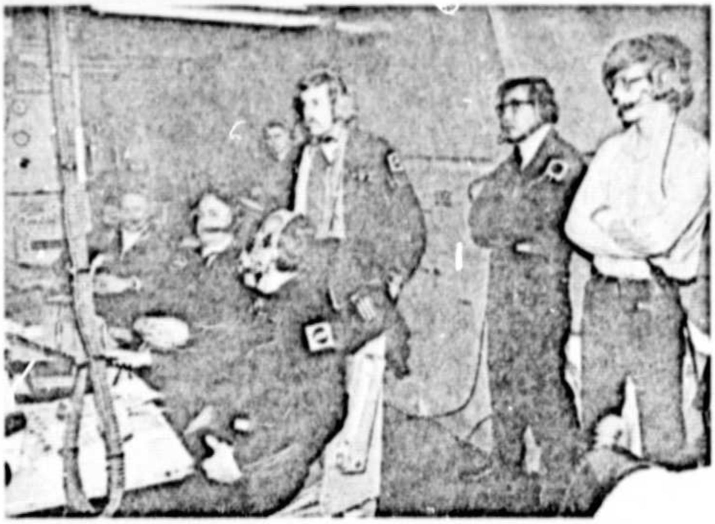

Left: Mars and Epsilon Geminorum on the television monitor screen, just after the occultation. Right: The KAO crew and author Craig Church (extreme right) watch the progress of the occultation on the monitor screen. Mission director Jim McLenahan is seated in the foreground.

KAO was approved, and preparations began immediately. We used the occultation photometer described in SKY AND TELESCOPE for December, 1975, page 356, for simultaneous observations at three wavelengths: 3700, 4500, and 7400 angstroms, in the ultraviolet, blue, and near infrared. The data were recorded digitally with a time resolution of 0.004 second to catch any abrupt variations, such as the momentary brightenings that were so evident during the disappearance and reappearance of Beta Scorpii when it was occulted by Jupiter in 1971.

Carl Gillespie is the C-141 project manager at NASA's Ames Research Center, Moffett Field, California, where the aircraft is based. Upon arrival, our main job was to modify the photometer for mounting on the telescope and for meeting rigid air safety requirements. Thanks to telescope technicians Bruce Kelley, Ben Horita, Don Oishi, and others, we were ready for a test flight two days before the occultation. The flight simulated as closely as possible the observing conditions that would be encountered during the actual occultation.

The operation of a large ground-based telescope often needs only one technician in addition to the astronomers doing the observing. But the complex systems of KAO require many more people: a flight crew of three, mission director, and operators for the telescope, star-tracker, and computer. In addition, an infrared radiometer measures the residual water vapor above the aircraft, to aid in interpreting infrared measurements. For our optical observations, the radiometer served as a sensitive detector of possible cirrus clouds. Two inertial navigation systems were used, and the precise position and velocity of the plane, along with other data, were written into the computer every two seconds.

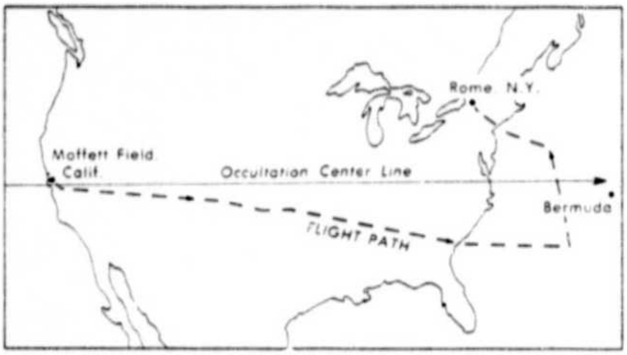

Right: The flight path of the aircraft was chosen to place the KAO on the central line of the occultation at the mid-time of the event.

The flight test went smoothly. After some initial adjustment, the tracker held Mars' image in the center of the photometer for long periods of time. And most important, the signals on our chart recorder were much smoother than during previous ground tests, the scintillation being much suppressed.

We took off from Moffett Field on the morning of April 7th and flew far enough east to be in total darkness at the time of the occultation and clear of the heavy air traffic along the East Coast. Since the telescope can be moved only a few degrees in azimuth, the position of Mars in the sky dictated that our course be nearly due north at the time of the occultation. Also, to make the most reliable determination of Mars' atmospheric composition, the apparent path of Epsilon Geminorum had to be perpendicular to the planet's limb. Hence, our course had to intersect the center line when the star was directly

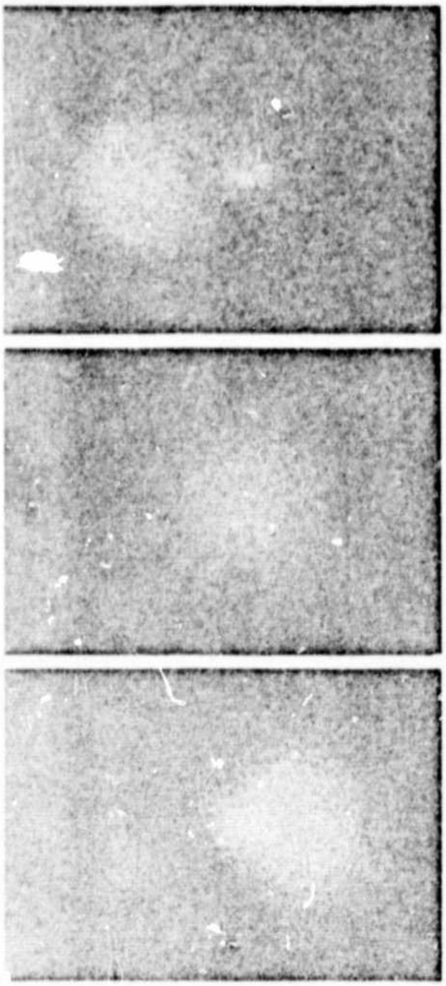

At Table Mountain Observatory, near Wrightwood, California, the 24-inch Cassegrain reflector was used by James W. Young to photograph the occultation. From the top: 0:53:50 Universal time, Mars is approaching Epsilon Geminorum; 0:54:40, a quarter minute after immersion; 0:59:40, the star has just emerged at the right of Mars. JPL-NASA photos.

behind Mars. Using final predictions from the English astronomer Gordon Taylor, navigator Bob Morrison prepared the flight plan.

Near Boulder, Colorado, we reset our clocks with WWV radio time signals. Since the transmitter was so near, timing errors due to propagation delay of the signals were minimized. We were flying away from the sun, and darkness came quickly as we crossed the eastern coastline. After some maneuvering to correct our arrival time at the center line, we turned northward.

Mars was acquired quickly by telescope operators Don Olson and Milo Reisner, then Harold Cauthen locked the tracker onto the image. A beam-splitter within the photometer directed some of the light to a television camera, and everyone could see the planet centered in the focal-plane aperture. Soon the image of Epsilon Geminorum entered and appeared to move slowly toward Mars. All systems were functioning perfectly, and Pete Kuhn reported that the infrared radiometer indicated clear sky above.

Finally, as seen on the monitor, the images of star and planet coalesced. Shortly thereafter, the chart-recorder pen dropped abruptly, traced a few irregular bumps, and then followed a smooth baseline. The occultation had begun.

Nearly three minutes later the light level increased for a few seconds, then dropped again. This was much too early for emersion, and a large "?" was written on the chart to indicate our astonishment. About 5¼ minutes after first contact Epsilon Geminorum emerged from behind Mars.

After landing at Griffiss Air Force Base at Rome, New York, we folded over the chart and lined up the immersion and emersion traces. The strange event occurred at mid-occultation — we had observed the *central flash*.

This phenomenon had eluded previous observers of occultations of stars by planets, because to see it one must be very close to the center line. To a visual observer on April 8th, the central flash should have appeared as a brightening all around the limb when the star was directly behind the center of Mars.

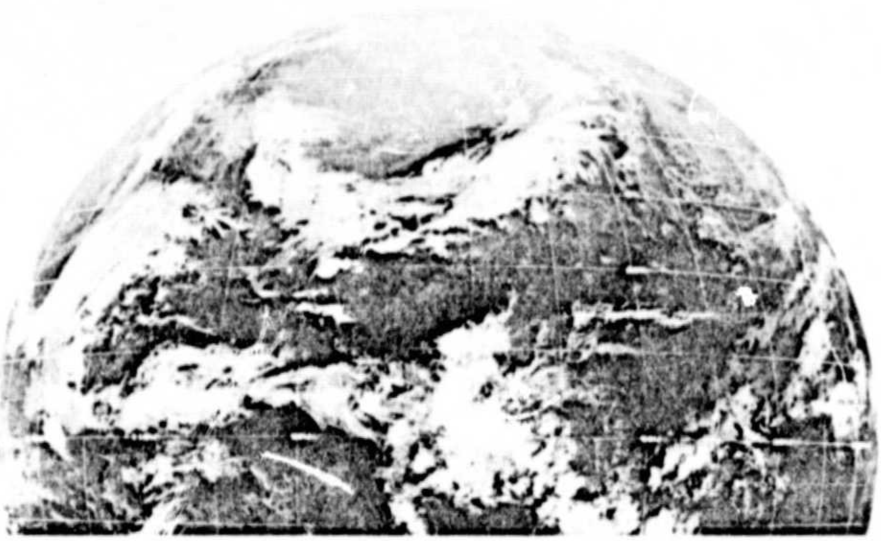

An infrared satellite picture of North America taken at 1:00 UT on April 8, 1976, shows the cloud distribution at the time Mars occulted Epsilon Geminorum. Cuba is near center; above it, a vast arc of clouds runs from the Dakotas to the Gulf States, then bends just off the Atlantic Coast toward Iceland. Except for thin haze, it is clear from Illinois to Maine, and nearly so in the Mountain States. National Oceanic and Atmospheric Administration photograph, courtesy Peter Kuhn.

This phenomenon was caused by the symmetrical refraction of light by the planet's atmosphere, which "focused" a portion of the light from Epsilon Geminorum. Further analysis should reveal whether diffraction by Mars' limb also had a role in creating the flash. In any case, the light of the central flash has probed much deeper regions of the Martian atmosphere than could be examined at immersion and emersion. Exactly what can be learned from this unique observation remains to be seen.

We are analyzing our data to obtain temperature profiles and to attempt to determine the relative abundance of argon and carbon dioxide in the Martian atmosphere. The presence of a substantial amount of argon has been suspected but not yet observed.

One curious feature of the light curves is that during immersion and emersion they show few of the spikes so prevalent at stellar occultations by Jupiter and Neptune. One reason for this is that the projected diameter of Epsilon Geminorum at Mars was approximately four kilometers, about half the scale height of the Martian atmosphere. (Scale height is the vertical distance in an atmosphere in which the density decreases by 1/2.718.) The presence of fewer spikes may also indicate that density variations in the atmosphere of Mars are less pronounced than in those of Jupiter or Neptune.

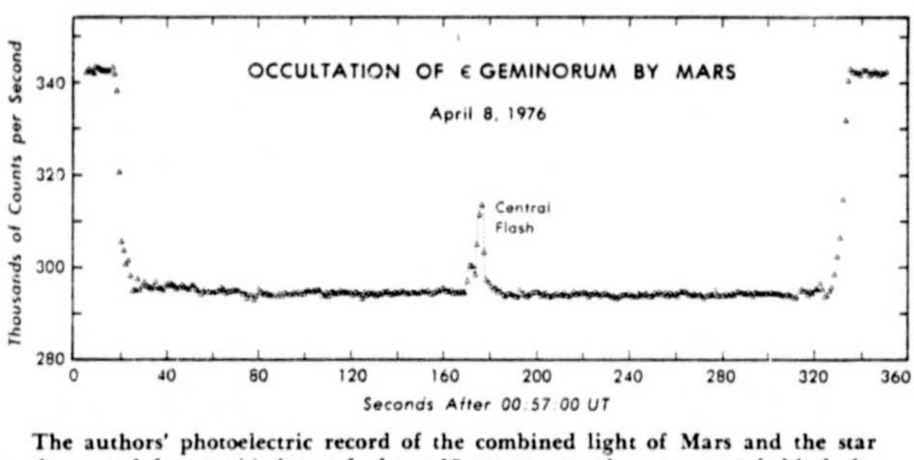

The authors' photoelectric record of the combined light of Mars and the star shows at left a rapid drop of about 15 percent as the star went behind the planet, and a corresponding rapid increase about five minutes later as the star emerged. The "central flash" is a phenomenon never before observed at an occultation, yet is theoretically predicted if the observer, the planet's center, and the star happen to lie exactly in line.

Reprinted from
4 February 1977, volume 195, pages 485-486

SCIENCE

Occultation of ϵ Geminorum by Mars: Evidence for Atmospheric Tides?

Abstract. *Temperature profiles of the martian atmosphere have been derived from airborne observations of the 8 April 1976 occultation of ϵ Geminorum. Within the altitude range from 50 to 90 kilometers, these profiles show peak-to-peak variations of 35°K with a vertical scale of 20 kilometers and represent evidence for strong tides in the martian atmosphere. However, more information is necessary to conclusively rule out a radiative explanation for the temperature variations.*

The martian occultation of ϵ Geminorum (visual magnitude = +3.1, spectral class G8Ib) on 8 April 1976 was observed with the 91-cm telescope aboard the National Aeronautics and Space Administration Kuiper Airborne Observatory, the first occultation observations made with this facility (*1*). High-quality light curves for both immersion and emersion were obtained simultaneously at three wavelengths (0.37, 0.45, and 0.75 μm) with a time resolution of 4 msec. A similar occultation of β Scorpii by Jupiter on 13 May 1971 yielded temperature and number density profiles of the jovian atmosphere (*2*), as well as a measurement of its He abundance (*3*). From our ϵ Gem occultation data we have obtained temperature, pressure, and number density profiles of the martian atmosphere and information about its composition from a differential refractivity measurement. Our result indicated that no more than 30 percent Ar (and N_2) is mixed with pure CO_2 (*4*) and is consistent with the low abundance of Ar and N_2 obtained by the Viking entry probe (*5*). In addition, we have obtained the wavelength dependence of the extinction of the martian atmosphere from the first observation of the central flash—a bright feature in the light curve that was recorded when ϵ Gem was aligned with the center of Mars (*1*). We report here the temperature profiles deduced from the occultation data, which were obtained above the martian coordinates 27°S, 331°W (immersion) and 28°N, 152°W (emersion) and cover an altitude range of about 50 to 90 km above the mean surface. These results are compared with those of Viking 1 (*5*) and with theoretical predictions of thermally driven tides in the martian atmosphere (*6*). The details of our observations, data analysis procedures, and other results are given elsewhere (*4*).

Temperature profiles were obtained from the occultation light curves with a new inversion procedure (*7*). This method is mathematically equivalent to standard inversion techniques (*2, 8*) but has the advantage that error bars (calculated from the known noise in the light curve) can be assigned to the temperature profiles. Thus we can have confidence in separating those features in the temperature profiles that are caused by the martian atmosphere from the variations arising from the noise in the light curve.

The temperature profiles obtained are given in Figs. 1 and 2. The profiles are for the light curves at 0.45 μm, the channel with the best signal-to-noise ratio; the profiles from our other two channels agree within their errors. The upper boundary condition for the inversion is determined by an isothermal fit to the upper part of the light curve, indicated by the shaded region at the top of Figs. 1 and 2. The temperatures and their error bars are obtained from the inversion calculation matched to the boundary condition. For each temperature point the error bars represent ± 1 standard deviation expected from the noise in the light curve. Neighboring temperature points agree better than the error bars because the noise affecting the points is correlated (*7*). The inversion calculation is terminated when the uncertainty in the lower base line of the light curve produces an error as large as the random error.

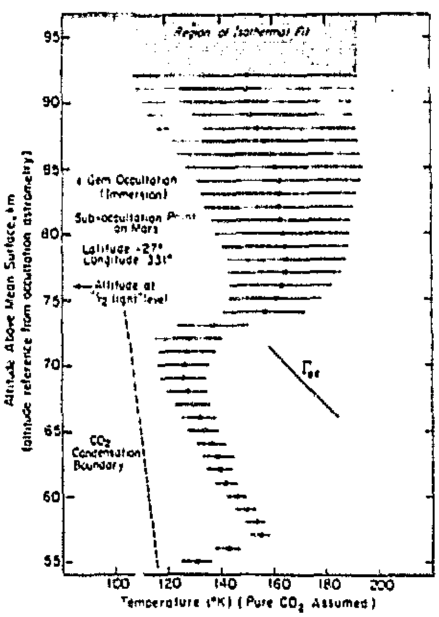

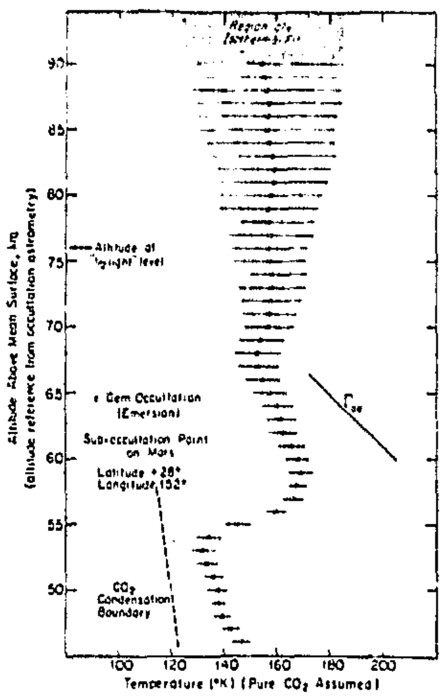

Fig. 1 (left). Temperature profiles for immersion. The plotted points and their error bars were obtained from the immersion light curve for a pure CO_2 atmosphere. A correction for the small amount of N_2 and Ar present would lower the temperatures about 3°K. The uncertainty in the altitude scale is ± 5 km, and an altitude of 65 km corresponds to a number density of 2.0×10^{14} cm^{-3}. The shaded region represents the uncertainty in the temperature obtained from the isothermal fit used to establish the boundary condition for the inversion calculation. The largest temperature gradients are subadiabatic ($\Gamma_{ad} = -5$°K km^{-1}). The wavelike structure strongly suggests the presence of tides in the martian atmosphere. At the time of the occulation, the martian subsolar latitude was + 19.2° and the planetocentric longitude of the sun (L_s) was 51.6°. Immersion occurred above the subocculation point on Mars at about 0330 local solar time. Fig. 2 (right). Temperature profile for emersion, which occurred above the subocculation point on Mars at about 1530 local solar time. For details, see the legend for Fig. 1.

Both the immersion and emersion profiles show peak-to-peak temperature variations of 35°K, much larger than variations expected from random noise. Temperature maxima occur at an altitude of about 55 to 60 km on both profiles. The mean temperature of the emersion profile is somewhat warmer than the mean for immersion. A temperature difference is to be expected from the difference in solar energy absorption, since the subsolar latitude is 19°N, close to the emersion latitude of 28°N, but 46° from the immersion latitude of 27°S. The mean temperatures for both profiles (as well as this quantity can be defined) agree with the mean temperatures obtained from Mars 6 (*9*) and Viking 1 entry data (*5*).

A striking similarity between the occultation temperature profiles and the Viking entry profile is the wavelike vertical structure with wavelength between two and three pressure scale heights and a peak-to-peak amplitude about 35°K at a number density of 10^{14} cm^{-3}, roughly eight scale heights above the 5-mbar pressure level. The wavelength and amplitude are in agreement with the general character of tidal waves predicted by Zurek (*6*) for clear (not dusty) conditions. Detailed comparison of temperature profiles, including phase information, with his predictions is not meaningful for several reasons. The details of profiles depend upon the amount and distribution of traces of dust in the atmosphere, and these factors are unknown. There may be significant additional forcing due to boundary layer convergence, neglected in Zurek's treatment. The large amplitude of the tides probably leads to instabilities and, as a result, to turbulence. Zurek pointed out that such turbulence would influence the structure of the tide but in a manner difficult to predict.

There are other possible explanations for the thermal structure. McElroy's detailed radiative equilibrium calculations (*10*) suggested that oscillations of temperature with height might occur near these levels on Mars because the concentration of (and solar absorption by) photodissociation products varies. Dütsch (*11*) discussed temperature variations in Earth's atmosphere caused by the stratification of photochemical products due to flow "fingering." Finally, aerosols have been observed by the Viking orbiter at heights as great as 40 km on Mars (*12*), and stratification into layers could lead to varying radiative heating with height. Purely thermal layering due to slowly varying (not tidal) large-scale flows is probably not a possibility, because radiative relaxation times are less than 1 day (*6*).

There is one point of disagreement between our data and Zurek's predictions, namely, the isothermal (not wavy) thermal structure above 70 km on emersion. However, radiative damping increases rapidly with height at these levels, and Zurek remarked that its influence is difficult to predict accurately.

We believe that the wavelength and amplitude of temperature variations shown by the data are best explained in terms of the existence of tides. A definitive test of this interpretation may be possible if several more temperature profiles of sufficiently high signal-to-noise ratio are available from other observers of the ϵ Gem occultation. These profiles, in conjunction with the Viking entry profiles, would provide information on the atmospheric temperature structure above different locations on Mars, which could be compared with the predictions of the tidal model.

J. L. ELLIOT, R. G. FRENCH
E. DUNHAM, P. J. GIERASCH
J. VEVERKA, C. CHURCH
CARL SAGAN

Laboratory for Planetary Studies, Cornell University, Ithaca, New York 14853

References and Notes

1. J. L. Elliot, E. Dunham, C. Church, *Sky Telescope* 52, 23 (1976).
2. W. B. Hubbard, R. E. Nather, D. S. Evans, R. G. Tull, D. C. Wells, G. W. van Citters, B. Warner, P. Vanden Bout, *Astron. J.* 77, 41 (1972); L. Vapillon, M. Combes, J. Lecacheux, *Astron. Astrophys.* 29, 135 (1973); J. Veverka, L. H. Wasserman, J. L. Elliot, C. Sagan, W. Liller, *Astron. J.* 79, 73 (1974). An extensive critical review of the results of the β Scorpii occultation by Jupiter is given by D. M. Hunten and J. Veverka [in *Jupiter*, T. Gehrels, Ed. (Univ. of Arizona Press, Tucson, 1976), p. 247].
3. J. L. Elliot, L. H. Wasserman, J. Veverka, C. Sagan, W. Liller, *Astrophys. J.* 190, 719 (1974).
4. A preliminary report containing temperature, pressure, and number density profiles, as well as the composition and extinction results for the martian atmosphere from the ϵ Gem occultation was presented to the Viking Project in June 1976. These results are being submitted for publication (J. L. Elliot, R. G. French, E. Dunham, P. J. Gierasch, J. Veverka, C. Church, C. Sagan, in preparation).
5. A. O. Nier, W. B. Hanson, A. Seiff, M. B. McElroy, N. W. Spencer, R. J. Duckett, T. C. D. Knight, W. S. Cook, *Science* 193, 786 (1976).
6. R. W. Zurek, *J. Atmos. Sci.* 33, 321 (1976).
7. This method is described by R. G. French, J. L. Elliot, and P. J. Gierasch (in preparation) and requires the three assumptions necessary for inversion of the light curves: (i) the refractivity gradients in the martian atmosphere are parallel to the local gravity gradient, (ii) ray crossing is not severe, and (iii) the atmosphere is near hydrostatic equilibrium. J. Africano, G. de Vaucouleurs, D. S. Evans, B. E. Finkel, R. E. Nather, C. Palm, E. Silverberg, J. Wiant, W. B. Hubbard, and J. R. Jokipii (*Astrophys. J.*, in press) have reduced their ϵ Gem occultation data obtained at McDonald Observatory, assuming turbulent temperature fluctuations added to an isothermal atmosphere.
8. J. Kovalesky and F. Link, *Astron. Astrophys.* 2, 398 (1969); L. H. Wasserman and J. Veverka, *Icarus* 20, 322 (1973).
9. V. V. Kerzhanovich, *Icarus*, in press.
10. M. B. McElroy, *J. Geophys. Res.* 74, 29 (1969).
11. H. U. Dütsch, *Adv. Geophys.* 15, 219 (1971).
12. M. H. Carr *et al.*, *Science* 193, 766 (1976).
13. We are extremely grateful to R. Cameron, C. Gillespie, J. McClenahan, and the rest of the staff of the Kuiper Airborne Observatory for their advice, cooperation, and assistance. We thank G. Taylor for supplying occultation predictions and the astrometric information needed for data reduction; A. T. Young, R. Zurek, R. Millis, L. H. Wasserman, and W. B. Hubbard for helpful discussions; and J. Goguen, M. Roth, and S. Arden for help in preparing for our observations. We thank D. M. Hunten, W. A. Baum, J. Pollack, S. I. Rasool, and N. Boggess for their interest and encouragement. We thank R. F. Fellows for prompt consideration of our grant proposal. Supported by NASA grant NSG-7243; partial support was also provided by NASA grants NGR 33-010-082, NGL 33-010-186, and NSG 7126, and by NSF grant MPS 75-06670. P.J.G. is supported in part by an Alfred P. Sloan Foundation research fellowship.

10 September 1976; revised 26 October 1976